*Modeling the exceptional south Foehn event (*Garmij*) over the Alborz Mountains during the extreme forest fire of December 2005*

Abbas Mofidi, Iman Soltanzadeh, Yadollah Yousefi, Azar Zarrin, Mohsen Soltani, Jafar Masoompour Samakosh, Ghasem Azizi, et al.

Natural Hazards
Journal of the International Society for the Prevention and Mitigation of Natural Hazards

ISSN 0921-030X

Nat Hazards
DOI 10.1007/s11069-014-1440-9

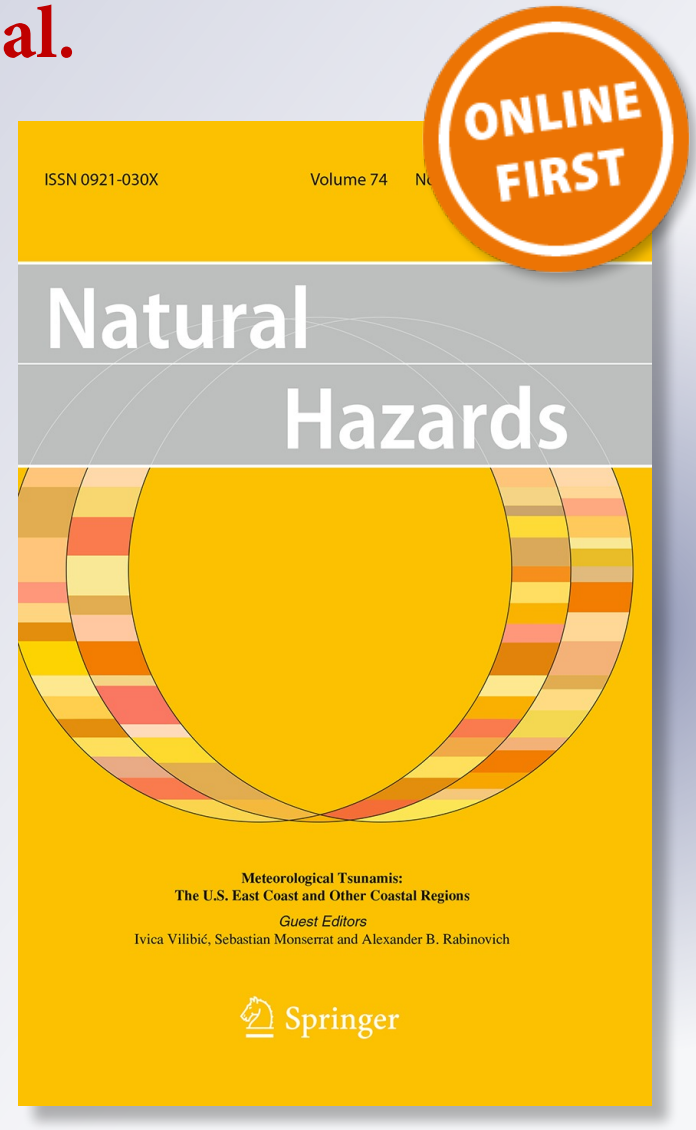

Springer

Nat Hazards
DOI 10.1007/s11069-014-1440-9

ORIGINAL PAPER

Modeling the exceptional south Foehn event (*Garmij*) over the Alborz Mountains during the extreme forest fire of December 2005

Abbas Mofidi · Iman Soltanzadeh · Yadollah Yousefi · Azar Zarrin · Mohsen Soltani · Jafar Masoompour Samakosh · Ghasem Azizi · Samuel T. K. Miller

Received: 27 September 2013 / Accepted: 14 September 2014

Abstract An exceptional southerly Foehn in the Alborz Mountains in northern Iran is investigated by using a combination of observations, reanalysis, and simulation data. A synoptic analysis is used as well as a high-resolution numerical modeling to clarify the Foehn event at different scales. The event resulted in an extensive and high-intensity fire in the Gilan and Mazandaran forests in northern Iran. The results indicate that a mechanically driven Foehn

A. Mofidi (✉) · A. Zarrin
Department of Geography, Ferdowsi University of Mashhad, Azadi SQ., Mashhad 9177948974, Khorasan-e- Razavi, Islamic Republic of Iran
e-mail: abbasmofidi@um.ac.ir

A. Zarrin
e-mail: zarrin@um.ac.ir

I. Soltanzadeh
Meteorological Service of New Zealand (MetService), Wellington, New Zealand
e-mail: iman.soltanzadeh@metservice.com

Y. Yousefi
Department of Geography and Urban Planing, Faculty of Humanity & Social Science, University of Mazandaran, Babolsar, Iran
e-mail: y.yousefi@umz.ac.ir

M. Soltani
Institute of Meteorology and Climate Research, Atmospheric Environmental Research (IMK-IFU), Karlsruhe Institute of Technology (KIT), Garmisch-Partenkirchen, Germany

J. Masoompour Samakosh
Department of Geography, Faculty of Humanities, Razi University, Kermanshah, Iran
e-mail: j.masoompour@razi.ac.ir

G. Azizi
Department of Physical Geography, Faculty of Geography, University of Tehran, Tehran, Iran

S. T. K. Miller
Department of Atmospheric Science and Chemistry, Plymouth State University, Plymouth, New Hampshire, USA

Published online: 23 September 2014

occurred in the Alborz Mountains during December 16–18, 2005. On the synoptic scale, the Foehn event occurred due to the presence of high pressure over the interior regions of Iran and lee cyclone over the southern Caspian Sea, with a strong south–north pressure gradient across the Alborz Mountains. In the mesoscale, the results suggest that mountain waves generated over the northern slopes of the Alborz Mountains are the primary source of the localized southerly wind maximum around the lee side of Alborz. A numerical simulation reveals that strong meridional surface pressure differences along with southerly flow, which is blocked upstream of the Alborz Mountains, result in higher nonlinearity and create large-amplitude vertically propagating mountain waves over the Alborz Mountains. The study also indicates that the wave-breaking region on the lee side with a critical level ranging from 600 to 400 hPa is responsible for reflecting the mountain wave energy back to the ground and for creating severe downslope wind (*Garmij*) in leeward side of Alborz Mountains. The Foehn event first appeared early on December 16, due to a wave-breaking at 550 hPa in western part of the Alborz Mountains.

Keywords Foehn · Forest fires · Downslope wind · Alborz Mountains · Mountain wave · WRF model

1 Introduction

Forest fires are a severe environmental hazard all over the world, caused by anthropogenic and natural forces. The development of forest fires is dependent upon three factors: fuel, topography, and weather. These three components interact, and the sum of their interactions determines fire behavior (Gorski and Farnsworth 2000). It is widely accepted that meteorological and climatic factors play a crucial role in fire behavior, affecting both the ignition and spread of wildfires (Pyne et al. 1996; Martin et al. 1997; Kunkel 2001). Meteorological variables alone, or in combination with vegetation and topographical parameters, are frequently used to develop fire risk indices. However, among three fire environmental components, the meteorological condition is the most variable component over time and is the most difficult one for the resource managers to interpret and predict (Whiteman 2000). On the other hand, mountains play a key role in shaping the local weather and climate in response to the large-scale forcing, and many of the processes that occur in mountainous landscapes have a potential to significantly affect the fire behavior in general (Sharples 2009). Over time, topography is the most constant of the three major components making up the fire environment, but it may vary considerably over space. Elevation, aspect and steepness of slopes, and landform characteristics must all be considered when assessing the influence of topography on weather and wildland fires (Whiteman 2000).

Most of topographically induced forest fires are associated with a cross mountain flows and Foehn-like occurrences. The latter of which are characterized by warm, dry winds on the lee side of mountain ranges. The warmth and dryness of the air are due to adiabatic compression of the air descending the mountain slopes. The combination of high wind speeds and low atmospheric moisture can cause rapid spreading of the fire. If dryness and drought is taken as a background state to the initiation of a widespread forest fire, the Foehn winds thus serve as episodic drivers of potential fire disaster (Sharples et al. 2010).

Foehn events are an important meteorological feature of the climate of regions situated in the lee of large mountain ranges (Barry 1992). For example, Ustrnul (1992) concluded that Foehn winds in the lee of the Polish Carpathians increased mean annual air temperature by about 1 °C and reduced relative humidity by approximately 10 %. The onset of

these topographically modified winds, referred to locally as the *Chinook* of the Rocky Mountains, the *Zonda* of the Andes, *Foehn* of the European Alps, and *Nor'wester* of southern Alps in New Zealand, is typically characterized by a rapid increase in air temperature and wind speed, and decrease in humidity (Brinkmann 1971). These conditions during winter and spring frequently accelerate snow-melting, which may result in flooding and avalanches, while during summer the onset of Foehn winds may trigger dust storms and significantly increase the risk of wildfires. Keeley (2004) found that the *Santa Ana* Foehn wind in southern California was a key driver in determining the area burned, overriding most other climate signals. Foehn winds also feature significantly as drivers of severe fire weather in Europe. Carrega (1991) discussed the occurrences of catastrophic fires near the French–Italian border driven by westerly Foehn winds, while Conedera et al. (1996) reported that in southern Switzerland, the main time for forest fires is during north Foehn occurrences. The Foehn winds have also been connected with elevated forest fire risk in Japan (Kondo and Kuwagata 1992) and certain parts of Korea (Lim 2002), despite the lower topography encountered there. They are also routinely mentioned in New Zealand fire weather assessments because of the effect that they have on humidity levels in the lee of the main mountain ranges (Salinger et al. 2000; Salinger and Porteous 2002). The strong gusty winds that are characteristic of Foehn conditions may exceed 50 ms^{-1} as reported by Reid and Turner (1997), Colle and Mass (1998), and Lilly and Zipser (1972). Such high wind speeds present a considerable hazard to buildings, utility structures, and aviation. When warm Foehn air overrides cooler surface-based air, strong temperature inversions occur that are effective barriers to the vertical exchange of atmospheric contaminants. During Chinook events, air quality in Calgary is two to four times worse than during non-Chinook weather (Nkemdirim and Leggat 1978). Foehn may also cause damage due to severe storms (Brinkmann 1974), snow-melting (Hoinka 1985), or high pollution levels (Hoinka and Rösler 1987), and it is of great importance to better predict the structure of the flow in the gaps and valleys and to diagnose the occurrence of flow splitting. In a study, Seibert et al. (2000) found that the onset of southerly Foehn winds in the Eastern Alps resulted in elevated ozone concentrations, especially in valleys at night when the usual nocturnal minimum was suppressed. They concluded that the south Foehn effectively transported photochemically produced ozone over the Alps from the Po basin into the valleys of the Foehn areas. As a result of such wide-ranging effects, detailed knowledge of Foehn events is essential for effective wind hazard and air quality management, and for utility, aviation, and agricultural operations. McGowan and Sturman (1996) and McGowan et al. (1996) studied the role of Foehn wind events in dust transport and dispersion, and regularly monitored wind speeds of 40–50 ms^{-1} as Foehn airflow was channeled down large river valleys. They also conducted another research to identify the role of surface heating and local topography on the occurrence of two Foehn wind events in Southern Alps (Lake Tekapo catchment). They found that the topographically modified Foehn is dependent on daytime surface heating and topographic channeling of flow in the catchment (McGowan et al. 2002). Hoinka (1985), in his study of Foehn airflow over the European Alps between Vicenza (Italy) and Munich (Germany), described mountain wave development, where peak gusts in the lee of the Alps were compatible with the observed wave amplitude and momentum flux.

Research has identified two main mechanisms for the occurrence of Foehn events around the world. The first mechanism appears when a moist flow rises on windward slope of a high mountain, and the latent heat of condensation is added to ascending air. Heat gained by this process is realized as warming at leeward stations when the air descends the leeward slope (Beran 1967; Whiteman 2000). This type of Foehn is referred to as

thermodynamically driven Foehn (Sharples et al. 2010). The second mechanism occurs when a low-level inversion on the windward side of a mountain is blocked, and the upper, drier layers descend to the ground on the leeward side (Beran 1967; Brinkmann 1974; Smith 1979). This type of Foehn is referred to as blocking Foehn or mechanically driven Foehn (Sharples et al. 2010). Instances of mechanically driven foehn winds have been studied by Cook and Topil (1952), Brinkmann (1973, 1974), Lockwood (1962), Seibert (1990), and Ustrnul (1992).

It is typical for the mechanically driven foehn to occur in association with a vertically propagating mountain wave (Brinkmann 1974; Klemp and Lilly 1975; Zängl 2003; Drechsel and Mayr 2008; Richner and Hächler 2013). A large-amplitude mountain wave may also produce very strong winds (*downslope winds*) that blow down the lee slope of the mountains (Smith 1979, 1985; Durran 2003a). In most downslope wind events, including the typical Foehn and Chinook, the onset of the downslope wind is accompanied by an increase in the surface temperature and a decrease in the dew point (Durran 2003b). Such a condition was observed when an extreme and devastating firestorm happened in southern California during the October 2003. The fires were caused by human activities and made worse by the *Santa Ana* winds. Huang et al. (2009) revealed that a wave-breaking region on the lee side of Sierra Nevada is responsible for reflecting the mountain wave energy back to the ground and for the creation of severe downslope (*Santa Ana*) winds. According to Huang et al. (2009), this Santa Ana wind was the second deadliest in California's history.

While most studies of Foehn events have focused on a few selected regions, such as the European Alps and Rocky mountains in the western most part of North America, similar events in northern Iran are not well represented in the meteorological literature. Many forest fires occur in Iran. For example, approximately 5,357 ha of Iran's forests burned during the period from 1990 to 1992, of which 2,155 ha were in the north of Iran (Jazirehei 1995). In addition, about 1,258 wildfire events occurred in the northern forests of Iran between 1998 and 2005, burning 7,623 ha of forests. According to some reports, forty-six Foehn events, locally known as *Garmij*,[1] caused wildfires from 1976 to 1990 over the northern regions of Iran and account for approximately 44 % of the total forest fires and other environmentally damaging events in the country (Parnian 1999). Shirzadi (1992) studied the synoptic and physical conditions of the Foehn phenomenon and its destructive effects using different techniques such as the Fransila coefficient, the Nesterov coefficient, and other methods, which use the reduction in humidity for the northern parts of Iran. She concluded that the domination of extra-tropical cyclones moving eastward through the Caspian Sea region should be the main reason for the occurrence of Foehn in the lee of the Alborz Mountains. She also noted that the number of hectares burned increases during Foehn wind events. Parnian (1999) investigated Foehn occurrence conditions in Gilan and Mazandaran provinces and obtained the same results.

To address the shortcomings of our understanding of Foehn winds in north of Iran and their impact on the occurrence of widespread forest fires, this study aims to document the features of an exceptional south Foehn event that occurred in December 2005 over Alborz Mountains and caused extensive forest fires in northern Iran. The event occurred in three provinces simultaneously and persisted for 3 days. According to local media report, a strong, dry, and hot southerly wind which dominated over Alborz Mountains created widespread and high-intensity forest fires in an area more than 155 ha in Gilan and Mazandaran provinces. A combined analysis of routinely available surface and upper air

[1] *Garmij* is a local name for a Foehn event in north of Alborz Mountains that means an *extremely warm wind*.

observations and a high-resolution simulation using the WRF model is used to study the physical mechanisms that created such an exceptional event.

2 Data and methods

The study is divided into three main parts. In the first part, we use observational data to clarify the Foehn event in the north of Iran. Local meteorological data used in this study were obtained from the Islamic Republic of Iran Meteorological Organization (IRIMO), and data describing the spatial distribution of forest fires were provided by the Natural Resources Administration Offices of Mazandaran and Gilan provinces. We use these data to give a brief presentation of the weather conditions on the north–south slopes of the Alborz Mountains.

In the second part, we apply a synoptic approach to investigate the regional-scale weather conditions during the Foehn event. For this purpose, we employ a combination of atmospheric reanalysis gridded data, satellite images, and a backward trajectory model output. Atmospheric gridded data were obtained from the National Centers for Environmental Prediction–National Center for Atmospheric Research (NCEP/NCAR) reanalysis dataset with 2.5° × 2.5° horizontal grid resolution (Kalnay et al. 1996). We also use precipitation data from Tropical Rainfall Measuring Mission (TRMM), with 0.25° × 0.25° horizontal grid resolution and 3-h time steps (Kummerow et al. 2000; http://trmm.gsfc.nasa.gov/). In addition, we use satellite images (Metosat5-IODC) obtained from the NEODAAS Geostationary Archive of the Dundee Satellite receiving station (www.sat.dundee.ac.uk). The Hybrid Single-Particle Lagrangian Integrated Trajectory (HYSPLIT) model (version 4.9), developed by NOAA ARL, is used to compute the backward trajectories discussed in this study (Draxler and Rolph 2011; Rolph 2011). Each backward trajectory was calculated for 48-h duration with three ending levels (50, 500, and 1,000 m AGL). The meteorological input for the trajectory model was the NCEP final analysis (FNL) dataset (reprocessed from NOAA's National Centers for Environmental Prediction Final Analysis data by the Air Resources Laboratory). The FNL input data were converted from the 1° latitude–longitude grid to hemispheric 129 by 129 polar stereographic grids with 190.5-km grid spacing by the ARL archiving program and available four times a day (00:00, 06:00, 12:00, 18:00 UTC). HYSPLIT uses archived 3-dimensional meteorological fields generated from observations and short-term forecasts (Stunder 1997).

In the third part, we use a numerical model to simulate the mesoscale circulation features associated with Foehn event over northern slope of the Alborz Mountains. For this purpose, we employ the Weather Research and Forecasting (WRF) modeling system (Skamarock et al. 2005; Skamarock and Klemp 2008) for the episode of December 16–18, 2005. The WRF–ARW model is a fully compressible, non-hydrostatic model with a hydrostatic option (Skamarock et al. 2005). The model uses a time-split small step for acoustic and gravity wave modes. The dynamics conserves scalar variables. A complete set of physics parameterizations is used. More information about model configuration and setup can be found in Table 1.

Topography, land use, and land–water mask datasets were interpolated from the USGS global covers with the appropriate spatial resolution for the domain. The USGS 24-category land-use/land-cover classification was considered representative of the dominant vegetation types in northern Iran. In this simulation, we used Noah land surface model, Noah LSM (Chen and Dudhia 2001). This scheme is coupled with a 4-layer soil temperature and moisture model, with canopy moisture and snow cover prediction. It includes

Table 1 WRF model configuration and setup in present study

Dynamics	Non-hydrostatic
Main prognostic variables	U, V, u10, v10, w, Qcloud, hgt, tk, tc, td, theta
Number of domain	Single domain
Central point of the domain	Central lat: 36.63N
	Central lon: 52.38E
Horizontal grid distance	2 km
Integration time step	90 s
Number of grid points	*X*-direction 490 points
	Y-direction 196 points
Map projection	Mercator
Horizontal grid distance	Arakawa C-grid (Skamarock et al. 2005)
Nesting	3 nested model domains (32, 8, and 2 km)
Vertical coordinate	30 sigma levels up to 14 hPa
Time integration	Third-order Runge–Kutta
Spatial differencing scheme	Second- to sixth-ordered centered differencing
Initial conditions	Three-dimensional real data (FNL: 1_91_)
Lateral boundary condition	Special options for real data
Top boundary condition	Gravity wave absorbing (diffusion and Rayleigh damping)
Bottom boundary condition	Physical or free slip
Cloud microphysics	WSM 6-class graupel scheme
Radiation scheme	Dudhia's short-wave radiation/RRTM long wave
Surface layer parameterization	Thermal diffusion scheme
Cumulus parameterization schemes	Betts–Miller–Janjic (Betts 1986; Betts and Miller 1986)
PBL parameterization	Land surface models (LSMs) (Han et al. 2008)

root zone, and other vegetation effects, drainage, and runoff, which provides sensible and latent heat fluxes to boundary-layer scheme. Three interactively one-way nested model domains are used with a horizontal mesh size of 32, 8, and 2 km, respectively, and all domains have 30 vertical levels. The corresponding grid points are 62 × 56, 178 × 112, and 490 × 196. The finest meshed domain covers an area about 980 km × 392 km and is centered at 36.63°N, 52.38°E (Fig. 1). The initialization date is 00:00 UTC, December 16, 2005, and the spin up of the model is 6.00 h. All simulations are terminated at 00:00 UTC, December 19.

3 Results and discussion

3.1 Foehn event description

3.1.1 Fire description

The fires under study took place on December 16–18, 2005 in the Gilan and Mazandaran forests, and during the 68 cases of forest fires, approximately 155 ha were affected. During the period under examination, one of the most significant forest fire events occurred over the northern forests of Iran and resulted in a great deal of irrecoverable losses (Table 2).

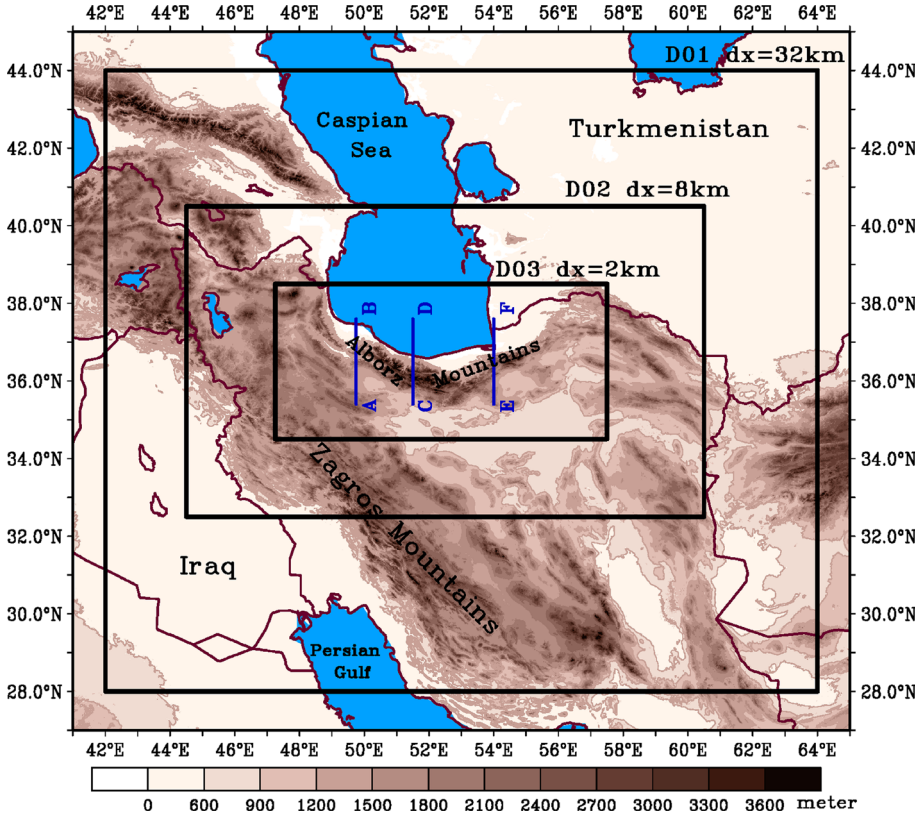

Fig. 1 Location and size of the three nested domains with background topography (*shaded*), used for WRF simulation. A 32–8–2-km nesting structure is applied for the spatial domains. *Three solid dashed lines* (*A–B*, *C–D,* and *E–F*) denote cross-sectional locations in Figs. 11, 12b, 13, 14, and 17

According to a local media report, the forest fires started at 4:30 GMT (1:00 local standard time (LST)) on Friday over high mountains. The report indicates that the forest fires started along with a strong warm and dry Foehn wind (*Garmij*), which occurred throughout the Alborz foothills. The Mazandaran forest fires occurred on a large scale, but the fire frequency in Gilan was greater than those of Mazandaran's, and the fires in some cases kept going for a few days. Forest fire distribution reached its maximum in eastern part of Gilan province as well (Fig. 2).

The forest fires on December 16 encompassed approximately 42 ha of the Gilan and Mazandaran forests. Fire sites were observed mostly in the eastern and western parts of Mazandaran, and the central areas of Gilan (Fig. 2). On December 17, at 28 sites in the two provinces, the fires spread further, encompassing nearly 83.5 ha of the forests. The distribution of fires on this day was more intense than the other days during the period. It was reported that there were fires at 26 sites in the two provinces covering about 24.6 ha on December 18, but eventually, during early December 19, the forest fires ceased in the Gilan and western Mazandaran provinces, even though four fires continued at sites in Mazandaran, threatening almost 8 ha of forests.

Table 2 Forest fire locations, frequencies, and burned areas on December 16–18, 2005 in the Gilan and Mazandaran provinces

	Sites	Date (December 2005)	Area (ha)	Forest fire sites		Sites	Date (December. 2005)	Area (ha)	Forest fire sites
1	Rasht	16, 17, 18	2.62	7	11	Amol	17	40	1
2	Rodsar	16, 17, 18	17.2	4	12	Behshahr	17, 18	25.6	5
3	Astara	17	2.15	3	13	Sari	16, 17, 18	5.7	7
4	Rodbar	17, 18	8.05	6	14	Neka	17, 18, 19	40.4	7
5	Talesh	17, 18	0.62	3	15	Noushahr	16, 18	1	2
6	Masal	18	0.5	1	16	Chamestan	16, 17, 18	1	1
7	Amlash	16, 17	1.2	2	17	Chalous	16, 17	0.1	4
8	Siahkal	17, 18	3.3	3	18	Ramsar	17	0.35	1
9	Shaft	18	4	2	19	Tonekabon	18	0.2	1
10	Lahijan	16, 18	0.42	8	–	–	–	–	–

The location of fire sites associated with the nearest meteorological station showed in Fig. 2

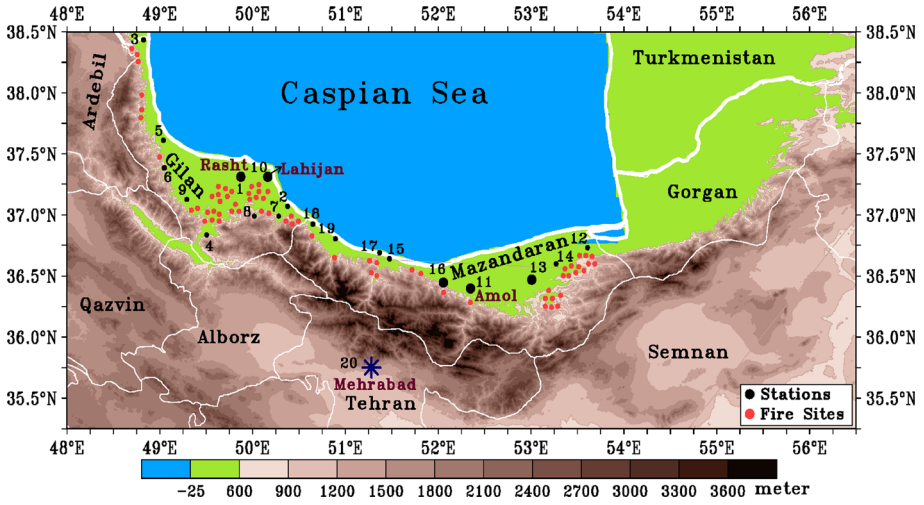

Fig. 2 Location of forest fire sites (*red circles*) and meteorological stations (*black closed circles*) used in the study and the underlying topography, and the Alborz Mountains in the north of Iran

3.1.2 Weather conditions in northern and southern slopes of the Alborz Mountains

Maximum temperature and minimum relative humidity at the Rasht, Lahijan, Amol (on the leeward side), and Tehran (on the windward side) stations on December 2005 are shown in Fig. 3 to demonstrate the variations in these elements as the most important indicator for differentiating a Foehn event from other days in December. It is obvious from Fig. 3a, b, c that the maximum temperatures in Rasht, Lahijan, and Amol stations, which are located leeward of the Alborz Mountains, show a downward trend at the beginning of December. Such a trend is to be expected with the onset of the cold season. The maximum temperature dramatically climbed (by more than 10 °C) while the minimum relative humidity value

shows a significant reduction (less than 25 %) in Rasht and Lahijan (as representatives for western part of Alborz) on December 16 and remains quite low during the period under study. The maximum temperature and minimum relative humidity diagrams of Amol station (as representative for middle and eastern parts) demonstrate similar behavior, even though the significant change in humidity and temperature occurred 1 day *later* on December 17 (Fig. 3). In addition, based on Table 3, a strong wind blew from the southwest at a high speed. It should also be noted that, on December 17, when forest fires reached their peak, all stations in the north side of the Alborz Mountains showed a strong wind from the south. It is worth mentioning that Sari station (on the east) had extremely weak maximum winds of only 4 knots, an indication that it was not in the direction of the Foehn swath. It may have been downstream of a possible hydraulic jump where the Foehn flow had already separated from the surface. Other characteristics of the observed weather elements are shown in Table 4. According to Table 4, in the middle and eastern parts of Alborz, a sudden drop in relative humidity and significant increase in temperature occurred 1 day after (December 17) these changes occurred in the western part.

Data from stations on the northern and southern slopes of the Alborz Mountains during the December 16–18 period were compared to quantify the dissimilarity in weather (particularly temperature) across the mountain range. Considering the thermodynamic forcing discussed above, it was expected that the weather conditions on the southern and western hillsides of the Alborz would be conducive for cloud formation and rainfall. In this regard, Table 5 shows the meteorological conditions for some stations south of the Alborz Mountains. Rainfall was reported at the stations south of the Alborz Mountains as follows: on December 17, Moallemkelayeh, Karaj, Tehran (Geophysics), Tehran (Chitgar), and Tehran (Mehrabad Airport) received 10.50, 5.60, 4.40, 8.0, and 3.50 mm (0.42, 0.22, 0.17, 0.32, and 0.14 inches), respectively. Also, on December 17 and 18, precipitation occurred at stations including Khodabandeh (14.0 and 2.50 mm), Khoramdareh (4.0 and 3.0 mm),

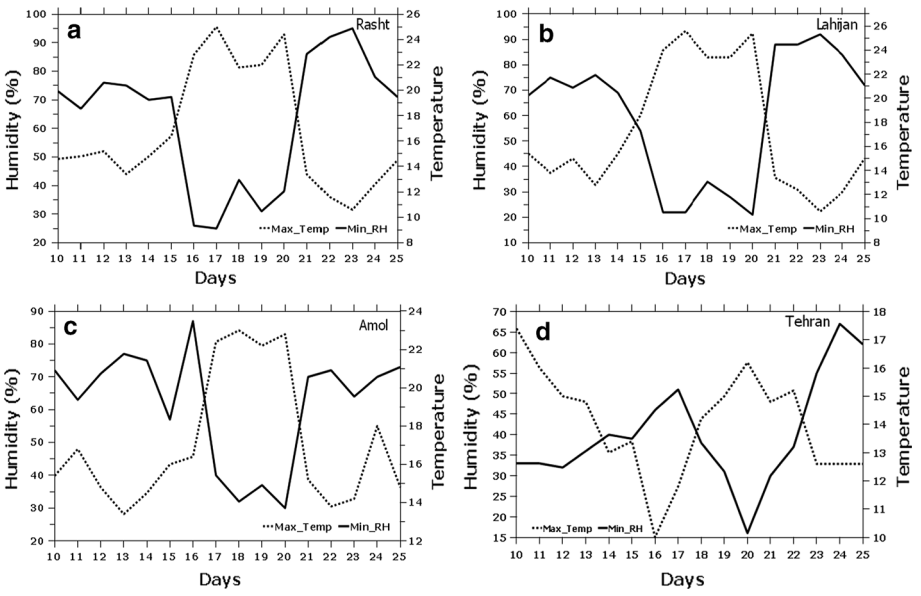

Fig. 3 Daily maximum temperature (*dashed line*, °C) and minimum relative humidity (*solid line*, %) for **a** Rasht, **b** Lahijan, **c** Amol, and **d** Tehran (Mehrabad) stations, December 10–25, 2005

Table 3 Wind characteristics in five stations during December 16–18, 2005

Stations	Date	Wind characteristics (Knot)					
		Mean	Highest values			Maximum wind	
		FF	DD	FF	Hours (GMT)	DD	FF
Rasht	December 16, 2005	9	180	19	12	210	23
	December 17, 2005	10	190	14	0	180	17
	December 18, 2005	2.8	90	6	12	90	6
Lahijan	December 16, 2005	4.6	180	23	12	180	27
	December 17, 2005	18	180	29	3	180	31
	December 18, 2005	**	**	**	**	140	7
Noushahr	December 16, 2005	10	210	31	21	220	34♀
	December 17, 2005	5	130	10	9	130	10
	December 18, 2005	2.8	360	6	9	360	6
Chamestan	December 16, 2005	8	180	10	15	180	10
	December 17, 2005	10	220	14	9	220	14
	December 18, 2005	4	50	4	9	**	**
Sari	December 16, 2005	4.3	150	12	3	150	12
	December 17, 2005	4	180	4	6	180	4
	December 18, 2005	2.3	360	6	3	360	6

All stations are located in north side of Alborz between foothills and Caspian Sea. See Fig. 2 for the locations

♀ A gusty wind is reported in Noushahr station on December 16, 2005

Symbol ** means data not available

Khalkhal (7.20 and 0.60 mm), and Avaj (8.0 and 17.4 mm). All these demonstrate a relatively extended rainfall occurrence on the windward slopes of the Alborz Mountains as an initial indicator of a moist upstream flow, which can be followed by descending air and the creation of a Foehn event on the leeward side. According to some studies, Foehn formation indices in the northern regions of Iran include southern and southwestern winds, warm and dry air, a very high visibility (corresponding to a low relative humidity), and strong winds with high directional variability (Shirzadi 1992; Parnian 1999). The above-mentioned conditions happened on December 16 and 17, 2005 in on leeside of the Alborz Mountains, as shown in Fig. 3 and Tables 3 and 4.

The rise in temperature and decrease in relative humidity in the north of Iran caused an unusually strong variation in temperature (maximum temperature) of more than 10 °C in stations such as Sari (23 °C), Tehran (12 °C), Garmsar (12 °C), Qazvin (9 °C), Rasht (25 °C), and Zanjan (10 °C). According to the stations' data, the Foehn event continued for 2 days. Based on the precipitation data, it is evident that the rainfall volume increased from hillside toward the peak of the mountain, with some precipitation falling as snow at elevations of 2,000 m and above.

By contrast, changes in temperature at Mehrabad, on the windward side of the Alborz Mountains, exhibited neither the magnitude nor the rates observed in the lee side (Fig. 3d). In fact, the temperature *decreases* to some extent over the examined period. In general, the observed temperatures on the upwind slopes of the Alborz are lower than those of observed on the northern side. In this period, the relative humidity along the southern slopes greatly *increased* in comparison with other times of the year. By contrast, the humidity

Table 4 Characteristics of weather elements for available stations in north side of the Alborz Mountains on December 16–18, 2005

Date	Stations	Visibility (km)			RH (%)		Temperature (°C)	
		Maximum	Minimum	Mean pressure (hPa)	Minimum	Mean	Maximum	Mean
December 16	Rasht	10	2.5	1,007.1	26	61.2	22.8	15.2
	Lahijan	10	10	1,003.7	22	69.4	24	15.4
	Noushahr	12	8	1,005.9	27	75.2	24.6	15.7
	Chamestan	–	–	–	72	83.3	19	12.0
	Amol	10	10	1,003.5	87	91	16.4	10.1
December 17	Rasht	20	10	1,007.4	25	31.8	25	19.9
	Lahijan	10	10	1,002.6	22	31.2	25.6	20.5
	Noushahr	12	10	1,006.9	44	62	22.2	18.3
	Chamestan	–	–	–	42	58.6	25	19
	Amol	10	10	1,003.1	40	64.6	22.4	17
December 18	Rasht	15	15	1,015.3	42	67	21.8	14.7
	Lahijan	10	10	1,009.9	34	54.8	23.4	17.2
	Noushahr	12	10	1,015.	49	67.1	21	14.1
	Chamestan	–	–	–	40	63	23.5	16.8
	Amol	12	10	1,011.9	32	60.6	23	15.5

dramatically *decreased* at stations on the northern side over the course of period. These figures indicate an influx of significantly drier air in the lee of the Alborz mountain range and are in contrast to those recorded on the upwind side at Mehrabad where the dew point remained at 6–8 °C (not shown).

The rawinsonde-derived thermodynamic diagram for Mehrabad airport, Tehran (Fig. 4), at five different times from 00.00 UTC December 15 to 00.00 UTC December 18, 2005 shows common characteristics on the upwind side of a Foehn event. A temperature inversion layer near the surface below 800 hPa level with a nearly dry-adiabatic layer above is present 1 day before Foehn onset. Additionally, wind barbs in Fig. 4a show that a northwesterly wind is dominant upwind of the Alborz at that time. Following the thermodynamic condition in subsequent profiles, drying increased over time and the wind direction reversed in the lower atmosphere, associated with a new enhanced temperature inversion layer in the middle troposphere at 00.00 UTC on December 16, 2005. Both the plotted thermodynamic profiles and computed stability indices (Showalter index and Lifted index, not shown here) show that the upstream flow on the windward side of the Alborz Mountains is statically stable on the first day of the Foehn event (Fig. 4b). It is obvious that the devastating forest fires on December 16 in Gillan and Mazandaran Provinces cannot be created by a thermodynamically driven Foehn, while the statically stable air on upwind side of Alborz Mountains is stratified and stable until later in the afternoon of December 16, 2005 (Fig. 4c, d). On the first day of Foehn event, a mid-tropospheric inversion layer is dominant on the upwind side of the Alborz Mountains, while the wind direction backed from west to the south. In early December 17, a moist southerly wind created a saturated

Table 5 Elements of weather in some stations on south side of Alborz on December 16–18, 2005

Stations	Date: December 2005	Rainfall (mm)	Maximum, RH (%)	Wind (knot)			Temperature (°C)			Pressure (hPa)
				Mean	DD	FF	Minimum	Maximum	Mean	
Tehran Mehrabad	17	3.5	77	2.3	130	6	7.2	11.8	9.5	1,015
Abali	17	9	88	0	210	5	−1	9.9	4.4	1,017.5
Chitgar	16	10.5	81	0.8	10	4	5.4	10.6	8	1,004.3
Dushantapeh	17	6.5	81	2.5	90	16	7.8	12.6	10.2	1,015
Firozkoh pollution	17	4.8	94	15	260		−3.4	−1	−2.2	1,015.6
Firozkoh	16	8.5	85	1.2	190	7	0.8	5.6	3.2	1,014.9
Imam airport	18	6.8	88	4.5	260	9	2.8	11.4	7.1	1,016.3
Geophysics	17	4.4	78	2	170	6	6.2	10.4	8.3	1,014.8
Karaj	18	5.6	89	5.6	130	12	4	11	7.5	1,014.6
North Tehran	17	5.7	92	1	150	5	5	9.6	7.3	1,014.8

mid-tropospheric layer over the upwind side of Alborz, while at that time, the temperature inversion layer completely disappeared from the area (Fig. 4e). Finally, this condition is changed at 00.00 UTC on December 18, when a moist and statically stable flow from the south is replaced by a dry northwesterly wind (Fig. 4f).

3.2 Synoptic analysis

In this section, we analyze the synoptic pattern that dominated during the period of the Foehn event. For this purpose, we generated the composites of several meteorological variables such as sea-level pressure, vector wind, relative vorticity, and geopotential height at multiple levels of the atmosphere, using the NCEP/NCAR reanalysis dataset, along with precipitation data, satellite images, and a backward trajectory model (HYSPLIT). The Foehn event under consideration was related to an elongated ridge, which penetrated from Afghanistan into the interior regions of Iran, and was associated with local high pressure over the Zagros Mountains during the first day of event (Fig. 5a, b). The westward propagation and strengthening of high pressure is related to a mid-tropospheric ridge, which developed east of a deep trough in the eastern Mediterranean during the Foehn event (Fig. 6a, b). It should be noted that, during the cold season, the area around the Arabian Peninsula is typically the location of a quasi-stationary subtropical ridge/anticyclone named the *Arabian Anticyclone*. According to some recent studies (Mofidi and Zarrin 2005; Raziei et al. 2011, 2013; de Vries et al. 2013), this ridge tends to intensify over the Middle East when a deep mid-tropospheric trough approaches the eastern Mediterranean, as it did in this case.

At the beginning of December 16, a deepening mid-tropospheric trough with northwest–southeast orientation approached the eastern Mediterranean, which, in turn, resulted in the northward and westward propagation of the *Arabian anticyclone* over the Middle East (Fig. 6a, b). Following the deep trough, the mid-tropospheric subtropical ridge intensified and extended an elongated ridge from Afghanistan to western Iran, which in turn established a continuous and extensive southerly flow at the regional scale (Fig. 5a, b). It seems that the interaction between the subtropical ridge over Iran and the deepening extra-tropical trough over eastern Mediterranean, in addition to the creation of a regional-scale southerly wind, was also the main driver for creating a topographically induced minor trough on lee side of the Alborz Mountains. In other words, the southerly wind induced by the interaction between extra-tropical and subtropical systems, after passing the Alborz Mountains, also created a minor trough in lee of the Alborz (Fig. 6a–d). Therefore, the cyclone that is seen in eastern Caspian Sea region (Fig. 5a–d) is a lee cyclone that formed due to the domination of topographically induced minor trough.

During the second day of the Foehn event, the low-level southerly wind transported moisture all the way from the southern water bodies around Arabian Peninsula to northern Iran. Figure 7b shows how the subtropical ridge/*Arabian Anticyclone* transported moisture from southern sea areas to the Alborz Mountains. The moisture was mainly transported from the Arabian Sea and Persian Gulf to the western half of Iran (Fig. 7a, b), where it ascended the windward slope of the high mountains, and resulted in precipitation in the mountainous areas of Iran. Satellite images of the associated cloud systems confirm that the moisture was originated from the south and also show that the cloud coverage was associated with the initiation of precipitation on a regional scale (Fig. 8). It should also be mentioned that on the first day of Foehn event, a high-pressure system that was located in the interior regions of Iran prevented the moisture transport to the north of Iran, even though a continuous southerly wind had been present during the whole period over the

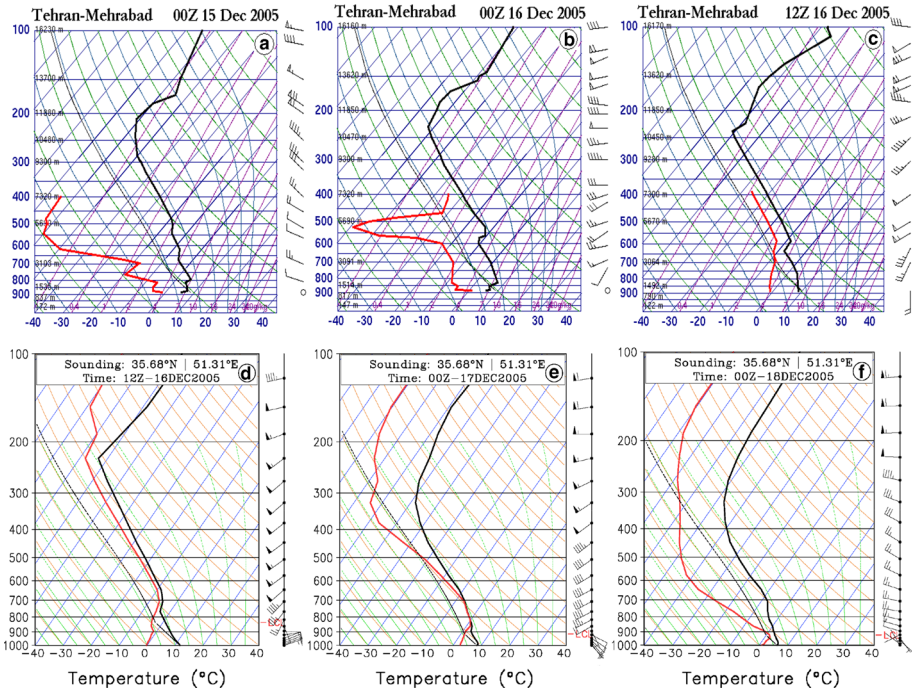

Fig. 4 Observed thermodynamic diagrams for Tehran (Mehrabad) valid at **a** 00:00 UTC December 15, **b** 00.00 UTC December 16, **c** 12.00 UTC December 16, and simulated thermodynamic diagrams (WRF outputs) for the same location valid at **d** 12.00 UTC December 16, **e** 00.00 UTC December 17, and **f** 00 UTC December 18, 2005. *Solid black line* denotes temperature and *solid red line* denotes dewpoint temperature. See Fig. 2 for the location

study area (Fig. 7a). However, the domination of a high pressure in the interior of Iran (Figs. 5, 7a) and a statically stable layer upstream of the Alborz Mountains (Fig. 4) prohibited the occurrence of large-scale precipitation in the north of Iran on December 16. According to meteorological reports provided by IRIMO, and precipitation data obtained from TRMM, on December 16, the western slopes of the Zagros Mountains received a maximum precipitation above 100 mm (3.94 inches), while the precipitation on the windward side and the summit of the Alborz Mountains exceeded 12 and 25 mm, respectively (Fig. 7c).

In this case, it seems that the continuous southerly wind at lower levels created sufficient conditions for the formation of a gravity wave on the summit or the northern slope of the Alborz Mountains, which strengthened the south–north pressure and vorticity gradients between the two sides of the mountains range (Fig. 8). Such a condition in the upstream flow, with stratified and statically stable layers (Fig. 4), along with a continuous southerly wind, can be favorable for the creation of upward-propagating mountain waves over the Alborz Mountains, which in turn can be followed by a strong downslope windstorm and mechanically driven Foehn on the lee side of mountains. At this time, the north side of the Alborz Mountains experienced descending air associated with low relative humidity and high potential temperature. Cooling in Mehrabad, and warming in Rasht and Lahijan on December 16 (Fig. 3), was due to a strong pressure gradient in the south–north direction

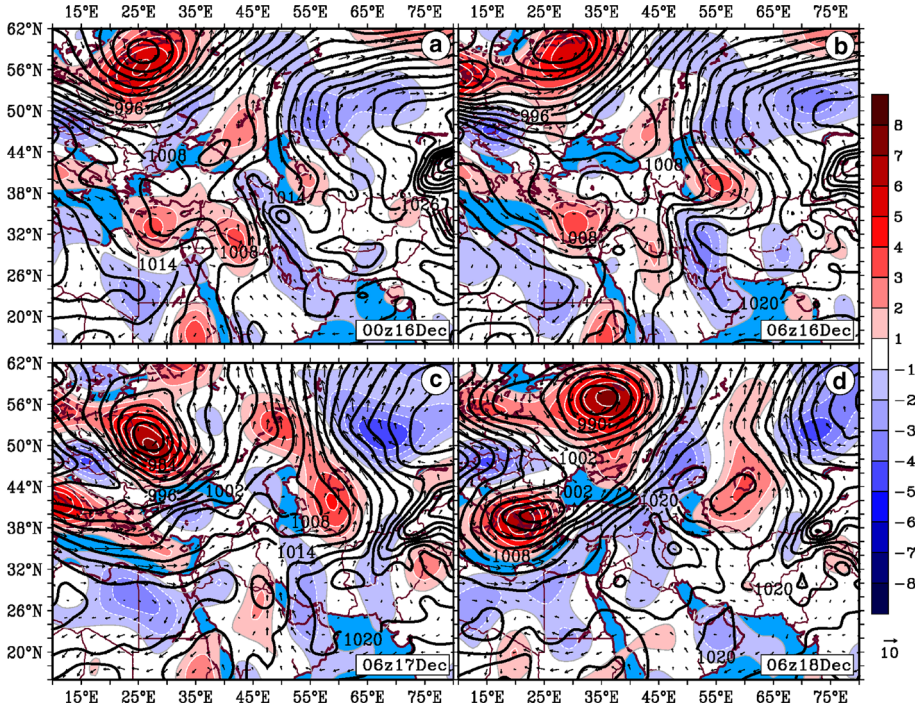

Fig. 5 Synoptic overview plots of sea-level pressure (contours, interval 3 hPa), vector wind (*arrows*, m s^{-1}), and relative vorticity (*shaded*, interval 10^{-5} s^{-1}) at 925 hPa. Results are valid at **a** 00:00 UTC December 16, **b** 06:00 UTC December 16, **c** 06:00 UTC December 17, and **d** 06:00 UTC December 18, 2005

over the Alborz Mountains, which was induced by the formation of high- and low-pressure centers to the south and north of the mountainous region, respectively (Fig. 8).

The 925 hPa level relative vorticity and vector wind, along with SLP at 00:00 and 06:00 UTC on December 16, 2005, are shown in Fig. 5a, b. A strong vorticity gradient between the interior regions of Iran and the Caspian Sea region in the north intensified a strong southerly wind across the Alborz Mountains. The strong southerly wind began when the pressure difference between the southern Caspian Sea (leeward) and interior of Iran (windward) in the south increased to 8 hPa at 6:00 UTC on December 16, which continued until 6:00 UTC on December 17, when the meridional pressure difference fell to less than 6 hPa (Fig. 8). The pressure gradient was maximized between December 16 (06.00 UTC) and December 17 (06:00 UTC) in the south–north direction, coinciding with the peak time of the Foehn activity. However, a rapid increase in the intensity of the southerly wind occurred on the leeward side of the Alborz Mountains at 12:00 UTC on December 16, as an abrupt decrease in the sea-level pressure appeared in windward side. The maximum pressure difference occurred at 00:00 UTC on December 17, when the pressure difference reached to 16 hPa between north and south sides of the Alborz Mountains (Fig. 8).

On the second day of the event, the satellite images indicate that the cloud systems gradually moved eastward (Fig. 9c–e), while a local- to regional-scale circulation in the lower atmosphere remained in control of the Foehn activity in the southern Caspian Sea region. Early on December 17, clouds disappeared over the western Alborz Mountains due to

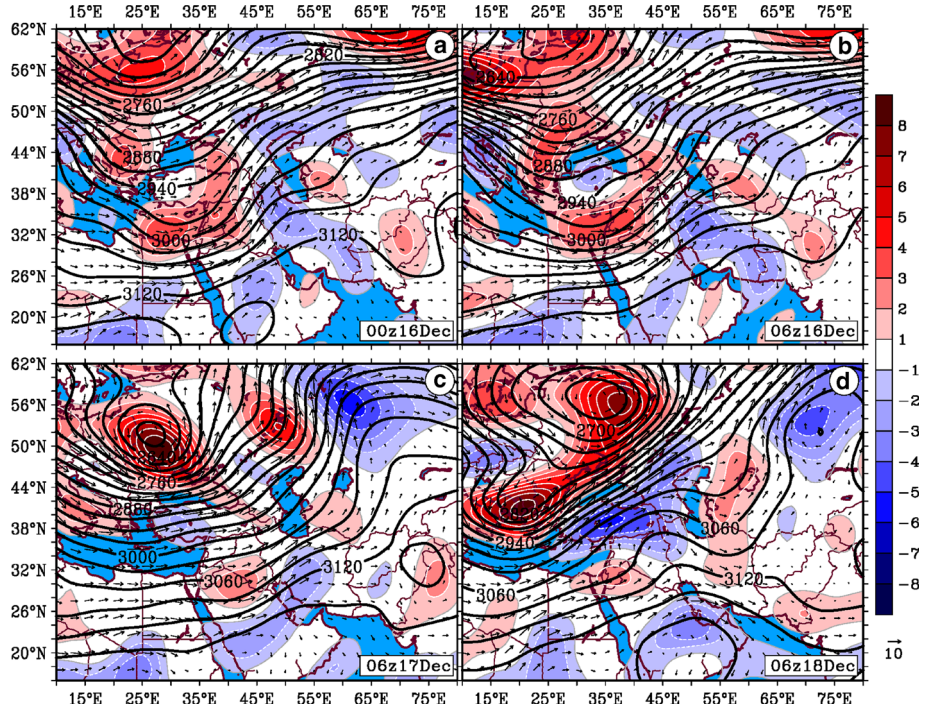

Fig. 6 Synoptic overview plots of geopotential height (*contours*, interval 30 gpm), vector wind (*arrows*, m s^{-1}), and relative vorticity (*shaded*, interval 10^{-5} s^{-1}) at 700 hPa. Results are valid at **a** 00:00 UTC December 16, **b** 06:00 UTC December 16, **c** 06:00 UTC December 17, and **d** 06:00 UTC December 18, 2005

a strong mid-tropospheric westerly wind, which approached the western part of the mountains (Figs. 7b, 9c). Early on December 18, the cloud systems completely disappeared from the Alborz Mountains region, as a strong westerly wind became established over the area (Fig. 9f). Finally, the Foehn event ended at 06:00 UTC on December 18, when the mid-tropospheric ridge moved to the west and stagnated over Iraq and eastern Turkey (Fig. 6d). At this time, in the lower atmosphere, a low-level elongated ridge appeared as a high-pressure center and moved to the west. After that, the wind changed from southerly to westerly, responding to the conditions in the mid-troposphere (Fig. 6d, 10b).

A backward trajectory Lagrangian model was applied to further investigate the weather conditions throughout the period of the study. The model was run for two leeward stations, Rasht and Sari, with ending times of 6:00 UTC on December 17 (peak time of Foehn activity) and 18:00 UTC on December 18, both with 48-h run duration. The result indicates that at the time of peak Foehn activity, the air parcels both in Rasht and Sari at all selected levels (50, 500, and 1,500 m AGL) originated from somewhere over the Persian Gulf (Fig. 10a-top). All trajectories descended to a level close to the ground (below 1,000 m AGL), indicating that before the parcels reached Zagros and Alborz Mountains, moisture was transported all the way across the interior of Iran under the influence of an anticyclone in the lower troposphere (*Arabian Anticyclone*). The backward trajectory cross section shown in Fig. 10a demonstrates that the parcel started to descend on the leeward side of the Alborz Mountains 6 h before the end of the model run (Fig. 10a-bottom). The result also

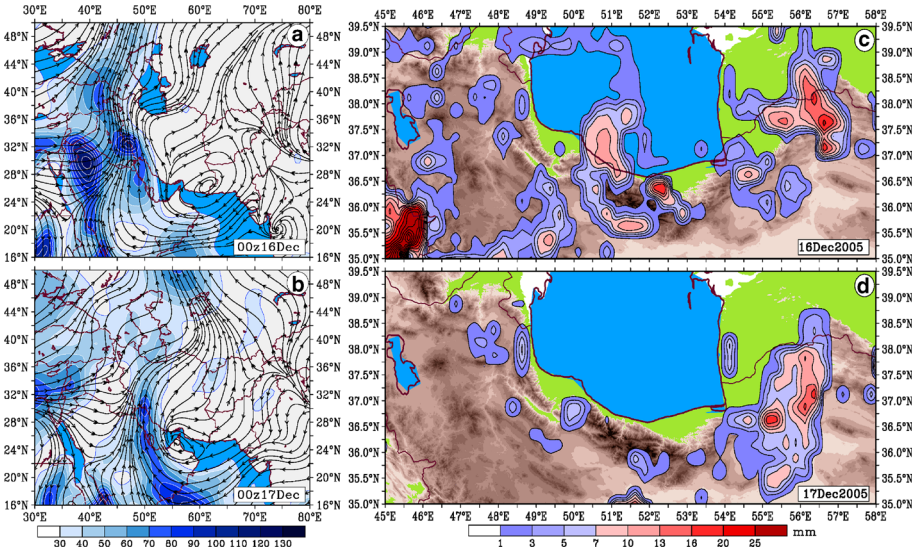

Fig. 7 Moisture transport (*shaded*, g s^{-1}) and streamlines at 925 hPa valid at **a** 00:00 UTC December 16, and **b** 00:00 UTC December 17, 2005. Tropical rainfall measuring mission (TRMM) accumulated precipitation (mm) for **c** December 16 and **d** December 17–18, 2005 (http://trmm.gsfc.nasa.gov/)

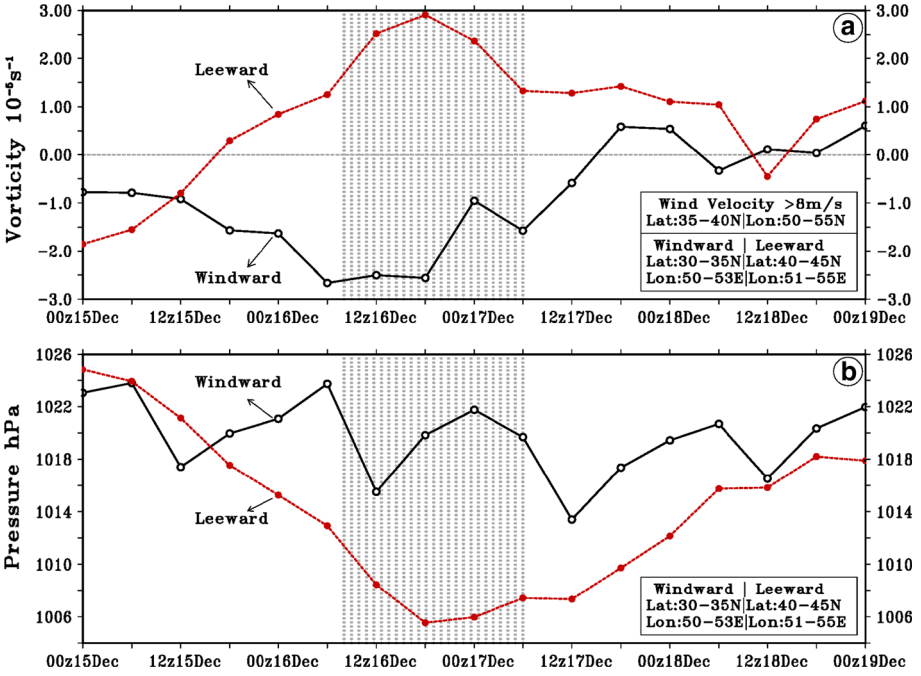

Fig. 8 **a** Relative vorticity ($\times 10^{-5}$ s^{-1}) and **b** sea-level pressure in windward (*solid black lines*) and leeward side (*red lines*) of the Alborz Mountains. *Hatched areas* show wind velocity greater than 10 m s^{-1}. *Boxes* in *lower right hand corner* of each figure provide the information for averaged area

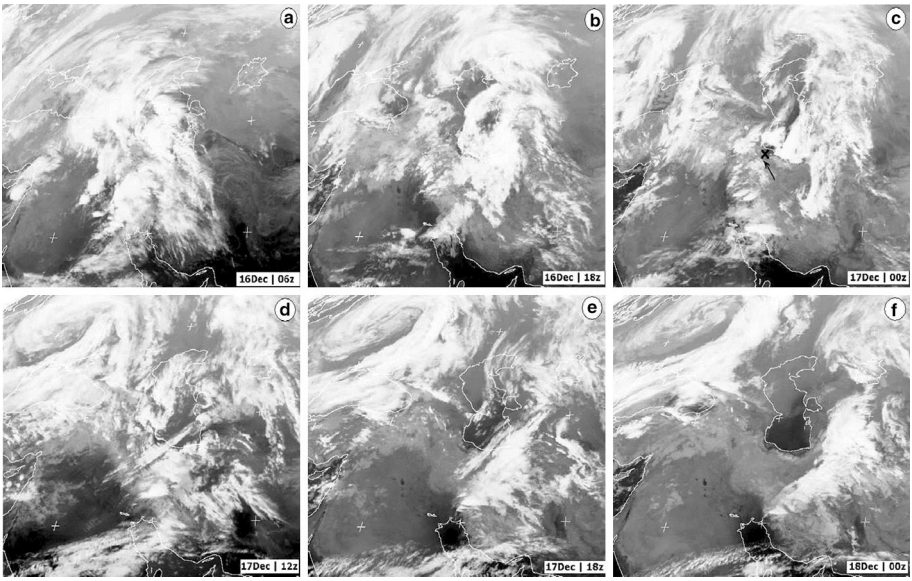

Fig. 9 Satellite (Metosat VISSR) images valid at **a** 06:00 UTC, **b** 18:00 UTC December 16, **c** 00:00 UTC, **d** 12:00 UTC, **e** 18:00 UTC December 17, and **f** 00:00 UTC December 18, 2005 (www.sat.dundee.ac.uk)

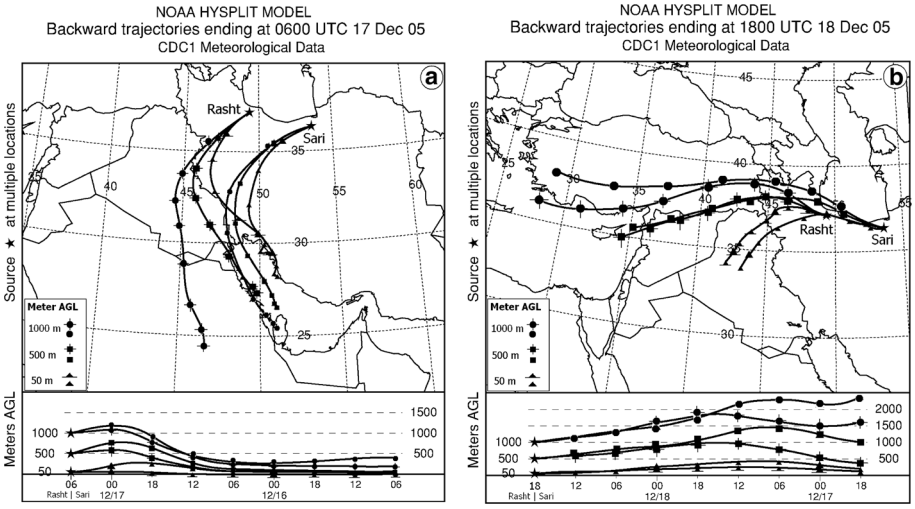

Fig. 10 HYSPLIT model backward trajectory outputs ending at **a** the peak time and **b** ending time of Foehn event. Model ran for 48 h and used a 6-h time steps (*nodes*). Plots demonstrate the individual air parcels at three levels [50, 500, and 1,000 m above ground level (AGL)] selected at Rasht and Sari stations. Backward trajectory cross sections are included in bottom of each figure for same levels

indicates that the long-range transport of air parcels coinciding with the ending time of Foehn activity (Fig. 10b-top) is completely different from the time of its peak. The parcels originated over the western Middle East, i.e., from northern Iraq to western Turkey, and in a range from near sea level to 700 hPa. It is important to note that there was no descending

air over the Alborz Mountains in this dominant westerly wind, even for parcels that originated from northern Iraq in the lower troposphere (Fig. 10b-bottom). The HYSPLIT model outputs confirm the synoptic analysis for the Foehn event discussed above.

3.3 Numerical simulation

In this section, the results of our numerical simulations are discussed. We start by focusing on the characteristics of the wind over the two sides of the Alborz Mountains.

The WRF simulation indicates that a strong southerly wind was initiated in the early hours of December 16 over whole area of northern Iran and continued until late on December 18 with some spatial and temporal variations. We applied Hovmöller diagrams (x–t diagrams) to clarify the evolution of the southerly wind over the area. Figure 11a, b indicates that the southerly wind started at the beginning of December 16 in the Alborz Mountains, and the duration, intensity, and extension of the southerly wind in the western part of Alborz were greater and stronger than it was in the eastern part. In the western part of Alborz, the intensity of the southerly wind reached a maximum between 06:00 UTC and 18:00 UTC on December 16, while in central and eastern parts, the highest intensity wind occurred little later, at 18:00 UTC on December 16 and persisted as a wildfire generator storm until 12:00 UTC on December 17. Now, it can be recognized why the extensive forest fires in Gilan, located in the western part of Alborz, started a little earlier in Mazandaran than in the eastern part. The WRF simulation also indicates that the southerly wind occurred for a shorter time in the eastern part than it did in the west and disappeared at 18:00 UTC on December 17 (Fig. 11a, b). The high-resolution model output reveals that the intensity of the southerly wind in the Alborz Mountains reached its maximum at a level around 900 hPa over the whole area, while its intensity decreased from west to east (Fig. 12a).

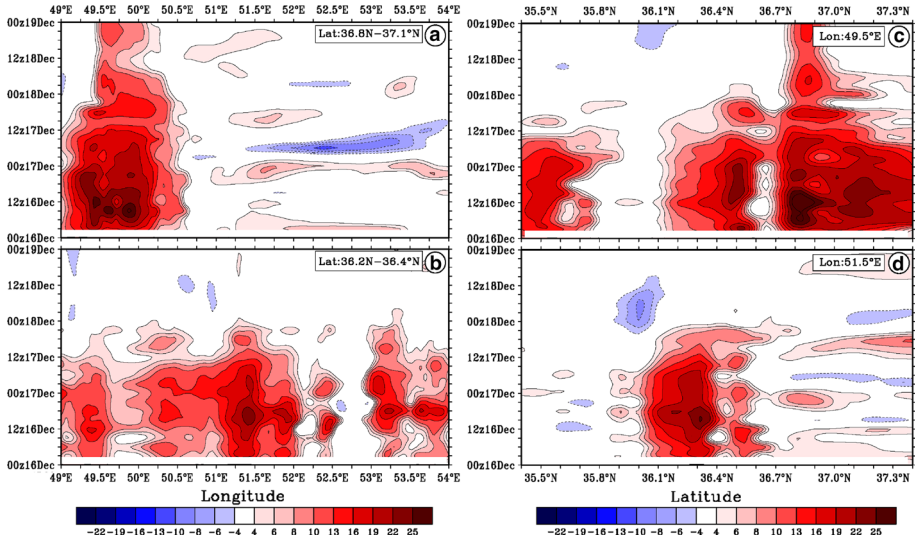

Fig. 11 Hovmöller diagrams of simulated meridional wind (increment: 2 m s^{-1}) at the surface in 6-h time steps for different geographical sections. **a**, **b** Averaged for latitudinal sections which the diagrams oriented across longitude and **c**, **d** Produced across latitude for 49.5°E (western Alborz) and 51.5°E (central Alborz), respectively

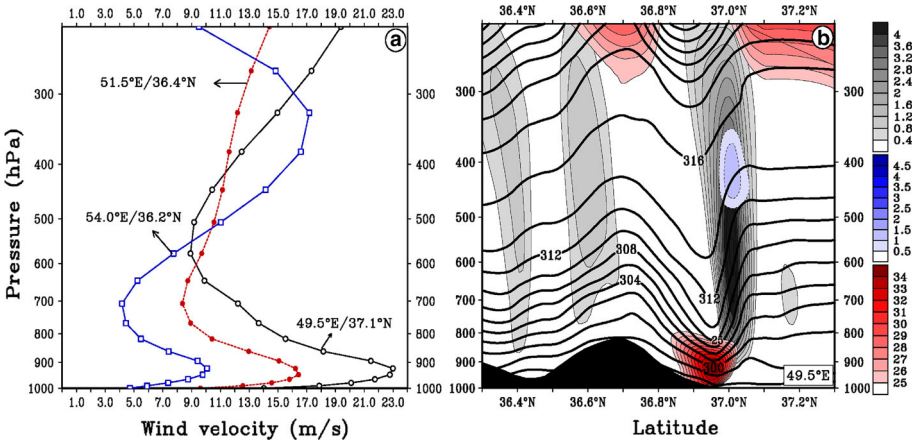

Fig. 12 **a** Vertical cross section of simulated meridional wind across leeward side of the Alborz Mountains averaged for main period of the Foehn occurrence (06:00 UTC December 16–12:00 UTC December 17). The *lines* are related to western (*open black circle*), central (*closed red circle*), and eastern (*open blue square*) Alborz, respectively. **b** Vertical cross section of potential temperature (*solid contours*, increment 2 K), updraft (*gray shaded*, increment 0.4 m s^{-1}), total cloud water mixing ratio (*blue shaded*, increment 0.5 g kg^{-1}), and wind velocity (*red shaded*, >25 m s^{-1}; increment 1 m s^{-1}) valid at 06:00 UTC December 16, 2005, derived from WRF simulations. The cross section is oriented across Alborz Mountains along line A–B indicated in Fig. 1 with underlying topography

Additionally, the model output indicates that in western part of the Alborz, the southerly wind penetrated as far north as the southern Caspian Sea, while in the central and eastern parts of the Alborz, it only appeared in a limited area on the lee slopes of high mountains and did not penetrate further to the north (Fig. 11c, d). This result may explain why the occurrence of forest fires in Gilan province in the west was greater and more distributed than in the central and eastern parts of the Alborz, where they were more concentrated during the Foehn event (Table 2; Fig. 2). At the beginning of December 16, domination of a strong continuous southerly wind associated with a stratified and statically stable layer in upwind slopes (Figs. 4, 12b) created a vertically propagating mountain wave on the Alborz Mountain summit (Fig. 12b) and then a strong downslope wind on leeward side of Alborz (Figs. 12, 13, 14). The simulation conducted here suggested that the gravity waves that excited over the northern slopes of the Alborz Mountains are the primary source of the localized southerly wind maximum on the lee side of the mountains. This leads to a strong subsidence of potentially warm air and thus a dry and warm Foehn wind on leeward side. Terrain-induced gravity waves significantly affect the resulting flow via momentum fluxes and pressure drag (Gaberšek and Durran 2004; Gohm and Mayr 2004; Gohm et al. 2008). Here, to fully understand the dynamics of nonlinear phenomena, such as upstream blocking, wave-breaking, and severe downslope winds, we need to take a nonlinear approach. It is worth mentioning that the basic dynamics of the severe downslope wind can be understood from the following two major theories (Lin 2007), (a) *Resonant amplification theory* (Clark and Peltier 1984) and (b) *Hydraulic theory* (Smith 1985), along with later studies on the effects of instabilities, nonlinearity, and upstream flow blocking. In *Hydraulic theory*, under certain stability, flow, and topographic conditions, large-scale instability can cause the mountain wave to undergo an abrupt change into what is termed a hydraulic flow (Whiteman 2000). Hydraulic flow is characterized by a region of wave-breaking aloft, a sudden jump in the streamline patterns, high wind speeds on the leeward

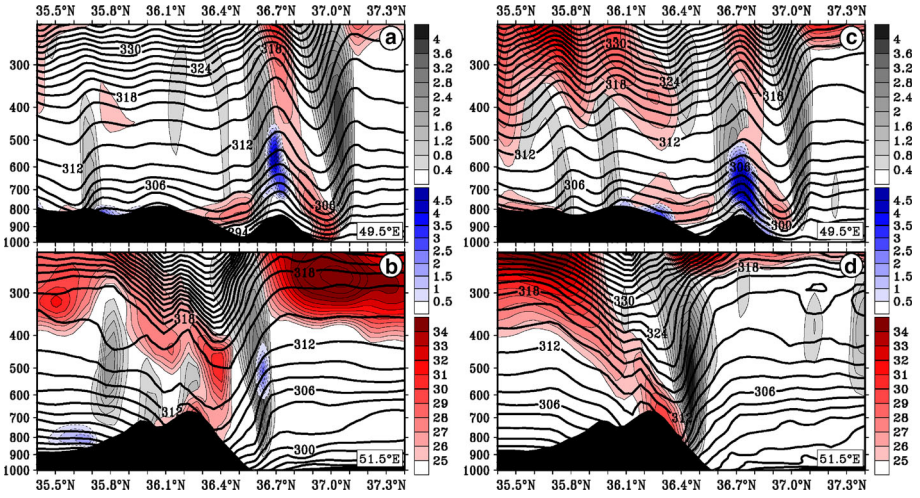

Fig. 13 Vertical cross sections of potential temperature (*solid black contours*, increment 2 K), updraft (*gray shaded*, increment: 0.4 m s^{-1}), total cloud water mixing ratio (*blue shaded*, increment: 0.5 g kg^{-1}) and wind velocity (*red shaded*, >25 m s^{-1}; increment: 1 m s^{-1}) valid at **a**, **b** 18.00 UTC December 16, **c**, **d** 00.00 UTC December 17, 2005, derived from WRF simulations. The cross sections are oriented across the Alborz Mountains along 49.5°E and 51.5°E, respectively. See Fig. 1 for location of the cross sections

slopes, a cavity at the bottom of the slope, and severe turbulence immediately beyond the cavity (Lilly 1978; Sharples 2009). According to *Resonant amplification theory*, the idealized nonlinear numerical experiments indicate that a severe downslope wind occurs after an upward-propagating mountain wave breaks above a mountain. The wave-breaking region is characterized by strong turbulent mixing, with a local wind reversal on top of it. Wind reversal level coincides with the critical level for a stationary mountain wave and thus is also referred to as the wave-induced critical level. Waves cannot propagate through the critical level and are reflected downwards. Thus, the wave-breaking region aloft acts as an internal boundary, which reflects the upward-propagating waves back to the ground and produces a severe downslope wind through partial resonance with the upward-propagating mountain waves.

Figure 12b shows a cross section of potential temperature, updraft motion, total cloud water mixing ratio, and wind velocity across the Alborz Mountains along transect AB at 06:00 UTC on December 16. It is obvious that a severe downslope wind with maximum wind velocity greater than 34 m s^{-1} at 900 hPa is created by a fairly large-amplitude and well-defined mountain wave, where a wave-breaking region aloft is reflecting the upward-propagating wave back to the ground and produced a severe down-lope wind in lee of the Alborz Mountains. Severe downslope winds hit the ground around 37°N and created an intense Foehn wind in the western part of the Alborz.

Based on numerical simulations, three distinct stages for the development of severe downslope winds, which in this study caused an exceptional south Foehn event, are evident (Scinocca and Peltier 1993; Lin 2007): (1) local static (buoyancy) instability develops when the wave steepens and overturns, thus producing a pool of well-mixed air aloft. Gray shaded area (updraft motion) in Fig. 12b shows such instability in a well-developed mountain wave over the Alborz Mountains at 06:00 UTC on December 16; (2) a well-defined large-amplitude stationary disturbance generates over the lee slope. At the same

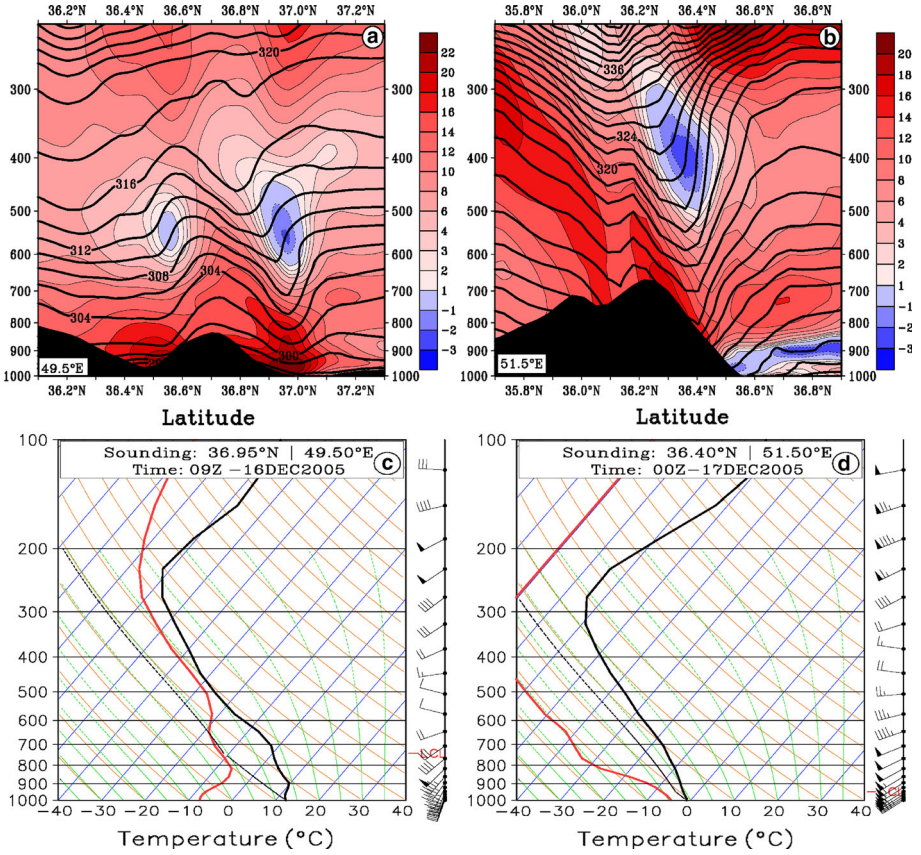

Fig. 14 **a**, **b** Vertical cross section of isentropes (*solid black contours*, K), and meridional wind component (*shaded*, m/s), for the western and central Alborz Mountains valid at 09.00 UTC December 16, and 00.00 UTC December 17, 2005, derived from WRF simulations. **c**, **d** Skew-T diagram and wind profile produced for wave-breaking regions as shown in (**a**) and (**b**)

time, small-scale secondary Kelvin–Helmholtz (K–H) (shear) instability develops in local regions of enhanced shear associated with flow perturbations caused by the large-amplitude disturbance; and (3) the region of enhanced wind on the lee slope expands downstream, eliminating the perturbative structure associated with the large-amplitude stationary disturbance (Fig. 12b). The K–H instability dominates the flow in this mature windstorm state. Thus, static instability helps explain the initiation of wave-induced critical level and the downstream expansion of the severe downslope winds.

Interpretation of wave effects in complex terrain is difficult, but some features can still be identified and explained. The flow in Figs. 12b and Fig. 13 appears to be nonlinear, evidenced by large-wave amplitudes, strong leeside acceleration, and wave-breaking. Indeed, all panels of Fig. 13 show nearly vertically oriented isentropes reminiscent of wave-breaking events.

To quantify the nonlinearity, we calculate the *non-dimensional mountain height* (also known as the *inverse Froude number*) for a volume upstream of the mountain (Reinecke and Durran 2008; Steinhoff et al. 2013):

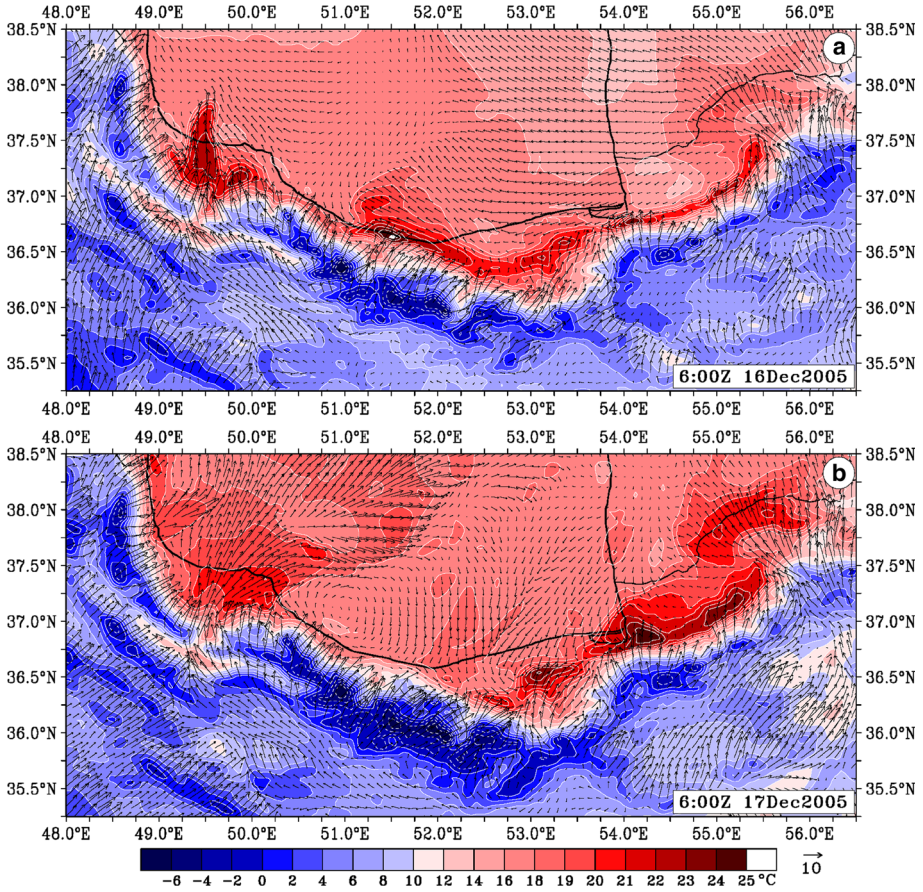

Fig. 15 Surface air temperature (*shaded*, °C) and vector wind at 1,000 hPa, valid at **a** 06:00 UTC December 16, and **b** 06:00 UTC December 17, 2005, derived from WRF simulations

$$M = \frac{Nh_{\mathrm{m}}}{U} \tag{1}$$

where U is the mean-state layer-average wind speed, N is the mean-state Brunt–Väisälä frequency, and h_{m} is the terrain height. Here, we calculate M over transect CD in Fig. 1 up to 2,100 m AGL. As recommended by Reinecke and Durran (2008), the average N in this layer is used to estimate the mean state in (1), rather than the bulk difference between the top and bottom of the layer. M is a measure of the nonlinearity of the flow, with an established threshold of 1.1 for continuously stratified, hydrostatic flow over a three-dimensional asymmetric Gaussian hill (Smith and Grønås 1993). This measure is only valid for the upstream, relatively undisturbed flow. A value of 1.47 is found at 00:00 UTC on December 17, indicating significant nonlinearity. In Fig. 12b, blocking is apparent upstream of the Alborz Mountains (36.2°N–36.6°N), with a large-amplitude mountain wave and acceleration in the lowest 2 km in the lee, where a very strong downslope wind of velocity greater than 34 m s^{-1} near the surface is seen to develop a Foehn event on the lee side.

The vertical structure of the flow over the Alborz Mountains is illustrated in Fig. 13. At 06:00 UTC on December 16, the Foehn event started with the onset of downslope wind in the north Alborz foothills (Fig. 11a, c), and an increased number of vertically propagating mountain waves occurred over the Alborz (Figs. 12b, 13). Mountain waves increased during the rest of the day and became large enough to create strong vertical motions (local static instability) on the top and adjacent leeward side of the Alborz Mountains (Fig. 13). Upward motion on the top of mountain reached its maximum between 12:00 UTC on December 16 and 00:00 UTC on December 17, when the mountain wave propagated vertically from the mountain top to the upper troposphere. Comparing flow features between western and eastern parts of the Alborz Mountains shows that the most severe downslope wind and most intense period of the Foehn activity occurred sometime early on December 16 (i.e., at 06:00 UTC) in the western part of the Alborz Mountains, while in the eastern part, the highest Foehn activity started about 12 h later (Figs. 13, 14, and 15).

Let us look again at the mountain wave simulation to clarify the wave-breaking regions in the Alborz Mountains. In Fig. 14a, b, isentropes and horizontal wind speeds are shown in solid black contours and shaded in red, respectively. By definition, the atmosphere becomes unstable when isentropes become vertical. These unstable regions hold the greatest potential for wave-breaking and its associated turbulence. When waves break, there is typically a region of reversed flow at the critical level. In this simulation, the critical level is observed in conjunction with mature, vertically propagating gravity waves. Note the region of small negative horizontal velocities directly above the mountain at about 550 hPa in western Alborz (Fig. 14a) and at 400 hPa in central Alborz (Fig. 14b). In both figures, the negative wind speeds depicted in blue, within the upper portion of the wave, correspond to the self-induced critical level. As shown in Fig. 14a, the strongest downslope winds typically develop directly beneath this critical layer. Mountain wave theory suggests that vertically propagating energy within the gravity wave reflects downward off of the critical layer and enhances the lee-side downslope wind speed.

The wind profiles in Fig. 14c, d show the critical level in different way. While in western and central Alborz the critical level is experiencing a weak northerly wind at 550 and 400 hPa, respectively, other pressure levels in top and down are experiencing a strong southerly wind at the same time (Fig. 14c, d).

Another feature appeared when the upward motion at the top of mountain reached its maximum and the mountain wave vertically propagated to the upper troposphere. The strong southerly wind during the second half of the first day was associated with strong

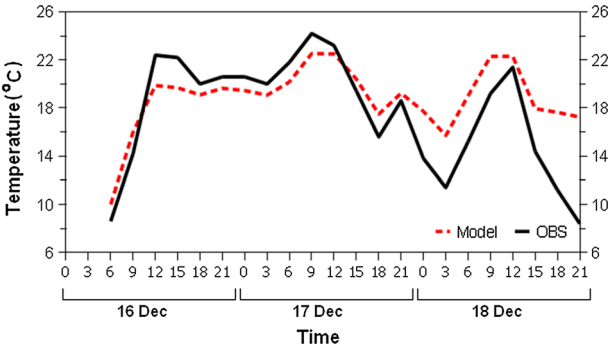

Fig. 16 Observed (*black line*) and simulated (*dashed line*) surface air temperature for the Rasht station (37°15′N–49°36′E). See Fig. 2 for the location

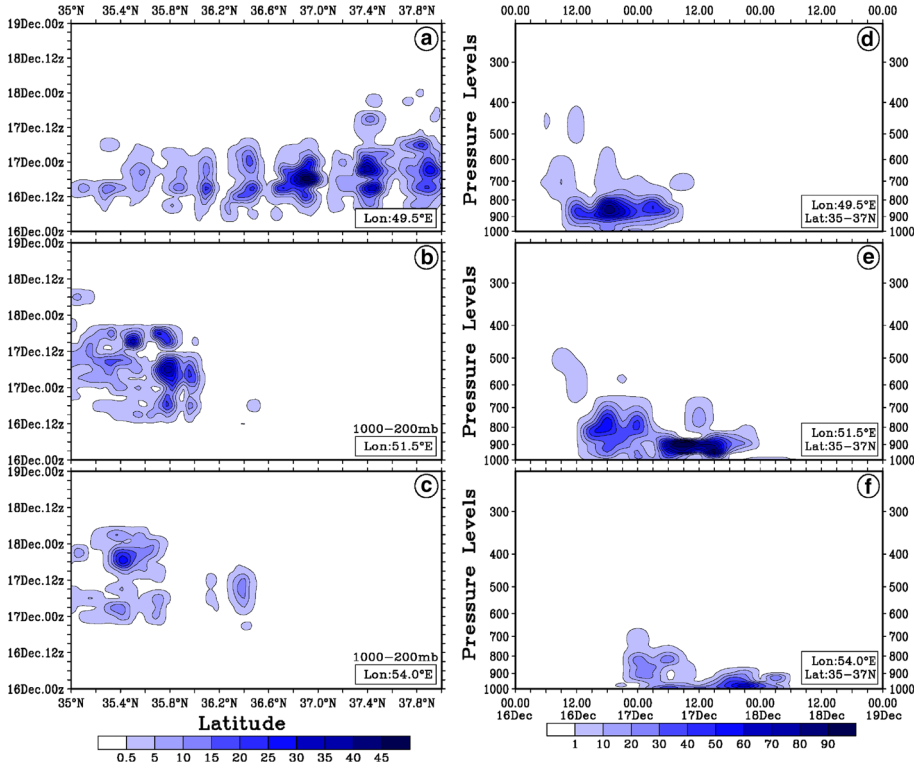

Fig. 17 Hovmöller diagrams of simulated total cloud water mixing ratio (g kg^{-1}) provided for the western (**a**, **d**), central (**b**, **e**), and eastern (**c**, **f**) Alborz Mountains. *Diagrams* in *left hand* indicate total amount of cloud water mixing ratio in troposphere (1,000–200 hPa), which are oriented across latitude. The *figures* in *right hand* indicate the conditions across pressure levels (y) and time (x)

meridional gradients in the surface pressure and vorticity (Fig. 9a, b), which were created by a large-amplitude mountain wave on the leeward side of Alborz. The result of this mountain wave-generated condition was a stronger downslope wind and a high surface temperature in the southern Caspian Sea area (Fig. 15). At that time, as illustrated in Fig. 15, ascending air on the windward side, and strong descending air on the leeward side of Alborz Mountains, created minimum and maximum surface temperatures on the top and leeward side of the mountains, respectively. A comparison of the atmospheric features on the western and eastern parts of the Alborz Mountains indicates that all features in the western part of the Alborz occurred about 1° farther north than in eastern part, due to local differences in size, height, and shape of the Alborz Mountains. Figure 15 confirms that the exceptional south Foehn event in the early hours of December 16 largely affected the surface air temperature in the western part of the Alborz Mountains (Fig. 15a), while on December 17, the influence of Foehn activity mainly caused a higher surface temperature in the eastern part (Fig, 15b).

To evaluate the model output, we compared simulated and observed surface air temperature for the same location (Rasht) in western part of Alborz (Fig. 16). As it is shown in Fig. 16, the surface air temperature in the high-resolution mesoscale model output is acceptable, and the observed and simulated temperature values are very similar during the whole period of the Foehn activity.

The WRF simulation also indicates that the Foehn event was accompanied by the formation of a stratified and precipitating cloud layer, which extended from the windward side of the Alborz up to the mountain top (Figs. 8b, c, 13, 17). Cloud layers mainly appeared over the area during the second half of the first day and first half of second day. At that time, a precipitating cloud layer could not penetrate to the leeward side in eastern part of Alborz (Fig. 17b, c), while in the western part, a deeper precipitating cloud layer penetrated to the north, all the way to the southern Caspian Sea basin (Fig. 17a, d). Additionally, the height of the cloud tops in the western part of Alborz Mountains reached 600 hPa (Fig. 17d), while in most of the eastern part, cloud tops were concentrated below 800 hPa. It is worth mentioning that the amplitude of mountain wave and the intensity of upward motion and downslope winds slightly decreased when mountain top clouds developed on western part of the Alborz Mountains at 18:00 UTC on December 16, 2005 (Fig. 13a, c). Jiang and Doyle (2009) showed that a deep moist layer reduces the stratification in the lower to middle troposphere and weakens mountain waves, but in our experiment, the amount of moisture at the mountain top was not enough to destroy the stratification of the mid-troposphere, even though the development of mountain top clouds slightly reduced the intensity of upward motion over the mountain as well as in Foehn activity on the lee slopes by affecting the upward propagation of mountain waves in the mid-troposphere.

Comparing cloud layers in the eastern and western parts of the Alborz Mountains indicated that the period of cloudiness in the central and eastern parts occurred later, and for a slightly longer of period of time in the east (Fig. 17b–f). The simulation also showed that, while the western part of the Alborz experienced a deeper and more widespread cloud system, cloudiness in the eastern part only occurred on the windward side of the Alborz Mountains and in a thinner layer. The cloud water mixing ratio was maximized both horizontally and vertically when the southerly wind in the western Alborz reached its highest velocity, so that between 12.00 UTC on December 16 and 00.00 UTC on December 17, cloud layers appeared at a height above 600 hPa (Fig. 17d). Cloud layers disappeared rapidly from a large area in the western part of Alborz at 12.00 UTC on December 17. Satellite images for the same time confirm this condition (Fig. 8d–f).

4 Conclusion

An exceptional strong southerly Foehn on the leeward side of the Alborz Mountains in northern Iran was investigated by using a combination of observations, reanalysis, and simulation data. We used a synoptic approach as well as a high-resolution numerical model (WRF) to quantify the Foehn event at different scales. The event was characterized by an unusually long Foehn period (almost 2 days) and extremely high temperatures on the leeward side of Alborz Mountains. This resulted in extensive, intense fires in the Gilan and Mazandaran forests in the northern Iran.

The Alborz Mountains are primarily aligned east to west and thus produce a limited barrier to westerly winds. Briefly, we can conclude that, with regard to east–west orientation of the Alborz Mountains and its location in subtropics, the mountain waves which were generated by the Alborz Mountains would be relatively rare and typically shallow, as Smith et al. (2007) mentioned for mountain waves activity in the Alps with similar conditions. In spite of low frequency, the Alborz Mountains are expected to have a few Foehn events causing topographically induced forest fires on leeward side each year. It happens when southerly wind-induced mountain waves dominate over the Alborz Mountains.

This study revealed that, on December 2005, the synoptic-scale circulation was largely responsible for the flow characteristics over the Alborz Mountains, and temperature variability during Foehn event depended on large-scale advection and the source region of the flow. At the synoptic scale, Foehn events frequently occur during the cold season, when the Alborz Mountains experience a strong pressure gradient in south–north direction, which in turn results from the simultaneous domination of an extra-tropical cyclone in the north and a strong high pressure in the south. The synoptic pattern that we identified for December 2005 confirms the result of previous studies (Shirzadi 1992; Azizi and Yousofi 2009; Azizi et al. 2013).

Comparing simulation results along with observations and synoptic analysis suggests that the fires which occurred in the Alborz Mountains during December 16–18, 2005 were caused by a mechanically driven Foehn. At the mesoscale, a high-resolution model simulation revealed that strong meridional surface pressure differences, along with a southerly flow which was blocked upstream of the Alborz Mountains, resulted in higher nonlinearity and created large-amplitude, vertically propagating mountain waves over the mountains. The large, long-lived mountain waves, in turn, created and intensified a downslope windstorm (Foehn wind) in the lee of the Alborz Mountains. Since the intensity of downslope wind is directly related to the intensity of the mountain wave, which in turn strongly depends on the upslope static stability, this experiment demonstrates the impact of statically stable, stratified upstream layer on the formation of Foehn winds and topography-induced forest fires on the leeward side of the Alborz Mountains. This result is in agreement with Smith (1985), Durran and Klemp (1987), Bacmeister and Pierrehumbert (1988), Huang et al. (2009), and Steinhoff et al. (2013), which indicated that the wave-breaking region on the lee side acts as an internal boundary to reflect the mountain wave energy back to the ground and creates severe downslope winds through partial resonance with the upward-propagating mountain waves (Lin 2007).

In our experiment, the volume of near-surface moisture was not enough to reduce the upslope blocking, and low-level moisture could not destroy the stratified and statically stable upstream layer until later time on December 17. Moreover, the experiment indicated that the increase in mountain top moisture at 18:00 UTC on December 16 tended to damp the upward-propagating mountain wave in western part of the Alborz Mountains, and it also tended to reduce downslope winds on the lee slopes. It seems that a mechanism illustrated by Jiang and Doyle (2009) and Rögnvaldsson et al. (2011) destroys static stability at the mountain top, so that the interaction between moist flow and topography leads to a destratification from the airflow and reduction in buoyancy frequency in middle troposphere (Smith et al. 2002).

The Foehn event persisted over the area until a mid-tropospheric trough destroyed the permanent southerly wind and changed it to westerly wind late on December 18.

Acknowledgments This research was supported by the Ferdowsi University of Mashhad (FUM) under grant 2/20173. The authors wish to express their appreciation to the Natural Resources Administration of Mazandaran and Gilan Provinces for providing forest fire reports. The daily meteorological data were provided by Islamic Republic of Iran Meteorological Organization (IRIMO). We also gratefully acknowledge the NOAA Air Resources Laboratory (ARL) for the provision of the HYSPLIT model and READY Web site used in this publication. Satellite images used in Fig. 8 were obtained from the NERC Earth Observation Data Acquisition and Analysis Service (NEODAAS), Geostationary Archive of the Dundee Satellite receiving station. The authors would like to thank the five anonymous reviewers for their valuable comments and suggestions to improve the quality of the paper.

References

Azizi Gh, Yousofi Y (2009) Foehn and forest fire in Mazandaran and Gilan provinces; a case study: the forest fire from December 16–21, 2005. Geogr Res 92:3–28 (in Persian)

Azizi Gh, Bourzoo F, Alijani B (2013) Synoptic analysis of forest fires in North of Iran; case study: Gilan and Golestan Provinces. J Hum Sci Modares 16(3):80–98 (in Persian)

Bacmeister JT, Pierrehumbert RT (1988) On high-drag states of nonlinear flow over an obstacle. J Atmos Sci 45:63–80

Barry RG (1992) Mountain weather and climate, 2nd edn. Routledge, London

Beran DW (1967) Large amplitude lee waves and Chinook winds. J Appl Meteorol 6:865–877

Betts AK (1986) A new convective adjustment scheme. Part I: observational and theoretical basis. Quart J Roy Meteor Soc 112:677–692

Betts AK, Miller MJ (1986) A new convective adjustment scheme. Part II: single column tests using GATE wave, BOMEX, ATEX, and Arctic Airmass data sets. Quart J Roy Meteor Soc 112:693–710

Brinkmann WAR (1971) What is a Foehn? Weather 26:230–239

Brinkmann WAR (1973) A climatological study of strong downslope winds in the Boulder area. NCAR Cooperative PhD thesis No. 27/INSTARR Occasional Paper No. 7, University of Colorado

Brinkmann WAR (1974) Strong down slope wind at Boulder Colorado. Weather 102:592–602

Carrega P (1991) A meteorological index for forest fire hazard in Mediterranean France. Int J Wildland Fire 1:79–86

Chen F, Dudhia J (2001) Coupling an advanced land surface–hydrology model with the penn state–NCAR MM5 modeling system. part I: model implementation and sensitivity. Mon Wea Rev 129:569–585

Clark TL, Peltier WR (1984) Critical level reflection and the resonant growth of nonlinear mountain waves. J Atmos Sci 41:3122–3134

Colle BA, Mass CF (1998) Windstorms along the western side of the Washington Cascade Mountains, part I: a high-resolution observational and modeling study of the 12 February 1995 event. Mon Weather Rev 126:28–52

Conedera M, Marxer P, Hoffmann C, Tinner W, Amman B (1996) Forest fire research in Switzerland. Part 1: fire ecology and history research in the Southern part of Switzerland. Int For Fire News 15:13–21

Cook AW, Topil AG (1952) Some examples of Chinooks east of the mountains in Colorado. Bull Am Meteorol Soc 33:42–47

De Vries AJ, Tyrlis E, Edry D, Krichak SO, Steil B, Lelieveld J (2013) Extreme precipitation events in the Middle East: dynamics of the active Red Sea trough. J Geophsy Res 118(13):7087–7108. doi:10.1002/jgrd.50569

Draxler RR, Rolph GD (2011) HYSPLIT (HYbrid single-particle lagrangian integrated trajectory) model access via NOAA ARL READY website http://ready.arl.noaa.gov/HYSPLIT.php. NOAA Air Resources Laboratory, Silver Spring, MD

Drechsel S, Mayr J (2008) Objective forecasting of Foehn winds for a subgrid-scale Alpine Valley. Weather Forecast 23:205–218. doi:10.1175/2007WAF021.1

Durran DR (2003a) Downslope winds. In: Holton JR, Pyle J, Curry JA (eds) Encyclopedia of atmospheric sciences. Elsevier Science Ltd, Amsterdam, pp 644–650

Durran DR (2003b) Lee waves and mountain waves. In: Holton JR, Pyle J, Curry JA (eds) Encyclopedia of atmospheric sciences. Elsevier Science Ltd, Amsterdam, pp 161–1169

Durran DR, Klemp JB (1987) Another look at downslope winds. Part II: nonlinear amplification beneath wave-overturning layers. J Atmos Sci 44:3402–3412

Gaberšek S, Durran DR (2004) Gap flows through idealized topography. Part I: forcing by large-scale winds in the non rotating limit. J Atmos Sci 61:2846–2862

Gohm A, Mayr GJ (2004) Hydraulic aspects of föhn winds in an Alpine valley. Q J R Meteorol Soc 130:449–480

Gohm A, Mayr GJ, Fix A, Giez A (2008) On the onset of bora and the formation of rotors and jumps near a mountain gap. Q J R Meteorol Soc 134:21–46

Gorski CJ, Farnsworth A (2000) Fire weather and smoke management. In: Whiteman CD (ed) Mountain meteorology; fundamentals and applications. Oxford University Press, New York, pp 237–272

Han Z, Ueda H, An J (2008) Evaluation and intercomparison of meteorological predictions by five MM5-PBL parameterizations in combination with three land-surface models. Atmos Environ 42:233–249

Hoinka KP (1985) Observation of airflow over the Alps during a Foehn event. Q J R Meteorol Soc 111:199–224. doi:10.1256/SMSQJ.46708

Hoinka KP, Rösler F (1987) The surface layer on the leeside of the Alps during Foehn. Meteorol Atmos Phys 37:245–258

Huang H, Lin Y-L, Kaplan ML, Charney JJ (2009) Synoptic-scale and mesoscale environments conducive to forest fires during the October 2003 extreme fire event in Southern California. J Appl Meteorol Climatol 48:553–579. doi:10.1175/2008JAMC1818.1
Jazirehei MH (1995) Forest and fires. J For Pasture 29:1–6 [In Persian]
Jiang Q, Doyle JD (2009) The impact of moisture on mountain waves during T-REX. Mon Weather Rev 137:3888–3906. doi:10.1175/2009MWR2985.1
Kalnay E et al (1996) The NCEP/NCAR 40-year reanalysis project. Bull Am Meteorol Soc 77:437–471
Keeley JE (2004) Impact of antecedent climate on fire regimes in coastal California. Int J Wildland Fire 13(2):173–182
Klemp JB, Lilly DK (1975) The dynamics of induced downslope winds. J Atmos Sci 32:320–339
Kondo J, Kuwagata T (1992) Enhancement of forest fires over northeastern Japan due to a typical strong dry wind. J Appl Meteorol 31:386–396
Kummerow C et al (2000) The status of the tropical rainfall measuring mission (TRMM) after two years in orbit. J Appl Meteorol 39:1965–1982
Kunkel KE (2001) Surface energy budget and fuel moisture. In: Johnson EA, Miyanishi K (eds) Forest fires: behavior and ecological effects. Academic Press, San Diego, pp 303–350
Lilly DK (1978) A severe downslope windstorm and aircraft turbulence event induced by a mountain wave. J Atmos Sci 35:59–77. doi:10.1175/1520-0469
Lilly DK, Zipser EJ (1972) The front range windstorm of 11 January 1972: a meteorological narrative. Weatherwise 25:56–63
Lim J-H (2002) Fire situation in Republic of Korea. Int For Fire News 26:61–65
Lin Y-L (2007) Mesoscale dynamics. Cambridge University Press, Cambridge
Lockwood JG (1962) Occurrence of föhn winds in the British Isles. Meteorol Mag 91:57–65
Martin D, Garcia Diez AC, Rivas Soriano L, Garcia Diez EL (1997) Meteorology and forest fires: conditions for ignition and conditions for development. J Appl Meteorol 36:705–710
McGowan HA, Sturman AP (1996) Regional and local scale characteristics of Foehn wind events over the South Island of New Zealand. Meteorol Atmos Phys 58:151–164
McGowan HA, Sturman AP, Owens IF (1996) Aeolian dust transportation and deposition by foehn winds in an alpine environment, Lake Tekapo, New Zealand. Geomorph 15:135–146
McGowan HA, Sturman AP, Kossmann M, Zawar-Reza P (2002) Observations of Foehn onset in the Southern Alps, New Zealand. Meteorol Atmos Phys 79(3–4):215–230
Mofidi A, Zarrin A (2005) Synoptic analysis of the nature of sudanese low (Case Study; December 2001 Storm). Sarzamin 6:24–48 (in Persian)
Nkemdirim LC, Leggat K (1978) The effect of Chinook weather on urban heat islands and air pollution. Water Air Soil Pollut 9:53–67
Parnian A (1999) Foehn formation conditions over the Gilan and Mazandaran provinces. M.S. Thesis, Islamic Azad University—North Tehran branch, Faculty of Marine Sciences, Department of Physics, Tehran
Pyne SJ, Andrews PL, Laven RD (1996) Introduction to wildland fire. Wiley, New York
Raziei T, Mofidi A, Santos JA, Bordi I (2011) Spatial and seasonal regimes of daily precipitation in Iran and large-scale atmospheric circulation. Int J Climatol 32:1226–1237. doi:10.1002/joc.2347
Raziei T, Bordi I, Santos JA, Mofidi A (2013) Atmospheric circulation types and winter daily precipitation in Iran. Int J Climatol 33:2232–2246. doi:10.1002/joc.3596
Reid S, Turner R (1997) Wind storms. Tephra 16:24–32
Reinecke PA, Durran DR (2008) Estimating topographic blocking using a Froude number when the static stability is nonuniform. J Atmos Sci 65:1035–1048
Richner H, Hächler P (2013) Understanding and Forecasting Alpine Foehn. In: Chow FK, De Wekker SFJ, Snyder B (eds) Mountain weather research and forecasting. Springer Atmospheric Sciences, Berlin, pp 219–260. doi:10.1007/978-94-007-4098-3_4
Rögnvaldsson O, Bao J-W, Ágústsson H, Ólafsson H (2011) Downslope windstorm in Iceland—WRF/MM5 model comparison. Atmos Chem Phys 11:103–120
Rolph GD (2011) Real-time environmental applications and display system (READY) website http://ready.arl.noaa.gov. NOAA Air Resources Laboratory, Silver Spring, MD
Salinger J, Porteous A (2002) Seasonal fire weather outlook January–March 2002. NIWA Rep. AK02003, National Institute of Water and Atmospheric Research, Auckland, New Zealand
Salinger J, Porteous A, Renwick J (2000) Seasonal fire weather outlook September–November 2000. NIWA Rep. AK00102, National Institute of Water and Atmospheric Research, Auckland, New Zealand
Scinocca JF, Peltier WR (1993) The instability of Long's stationary solution and the evolution toward severe downslope windstorm flow. Part I: nested grid numerical simulations. J Atmos Sci 50:2245–2263
Seibert P (1990) South foehn studies since the ALPEX experiment. Meteorol Atmos Phys 43:91–103

Seibert P, Feldmann H, Neininger B, Baumle M, Trickl T (2000) South Foehn and ozone in the Eastern Alps—case study and climatologically aspects. Atmos Environ 34:1379–1394

Sharples JJ (2009) An overview of mountain meteorological effects relevant to fire behaviour and bushfire risk. Int J Wildland Fire 18:737–754

Sharples JJ, Mills GA, McRae RHD, Weber RO (2010) Foehn-like winds and elevated fire danger conditions in south-eastern Australia. J Appl Meteorol Climatol 49(6):1067–1095

Shirzadi H (1992) The study of physical and synoptic condition of Foehn events and its destructive effects in Iran. M.S. Thesis, University of Tehran, Institute of Geophysics, Tehran

Skamarock WC, Klemp JB (2008) A time-split nonhydrostatic atmospheric model for weather and forecasting applications. J Comp Phys 227:3465–3485. doi:10.1016/j.jcp.2007.01.037

Skamarock WC, Klemp JB, Dudhia J, Gill DO, Barker DM, Wang W, Powers JG (2005) A description of the advanced research WRF Version 2. NCAR Technical Note NCAR/TN–468 + STR. http://www.mmm.ucar.edu/wrf/users/docs/arw_v2.pdf

Smith RB (1979) The influence of mountains on the atmosphere. Adv Geophys 21:87–230

Smith RB (1985) On severe downslope winds. J Atmos Sci 42:2597–2603

Smith RB, Grønås S (1993) Stagnation points and bifurcation in 3-D mountain airflow. Tellus 45A:28–43

Smith RB, Skubis ST, Doyle JD, Broad A, Kiemle C, Volkert H (2002) Mountain waves over Mt. Blanc: influence of stagnant boundary layer. J Atmos Sci 59:2073–2092

Smith RB, Doyle JD, Jiang Q, Smith SA (2007) Alpine gravity waves: lessons from MAP regarding mountain wave generation and breaking. Q J R Meteorol Soc 133:917–936. doi:10.1002/qj.103

Steinhoff D, Bromwich DH, Monaghan A (2013) Dynamics of the Foehn mechanism in the McMurdo Dry Valleys of Antarctica from Polar WRF. Q J R Meteorol Soc 139(675):1615–1631. doi:10.1002/qj.2038

Stunder BJB (1997) NCEP model output—FNL ARCHIVE DATA, TD-6141. Prepared for National Climatic Data Center (NCDC). This document and archive grid domain maps are also available at http://www.arl.noaa.gov/ss/transport/archives.html

Ustrnul Z (1992) Influence of foehn winds on air temperature and humidity in the Polish Carpathians. Theor Appl Climatol 45(1):43–47

Whiteman CD (2000) Mountain meteorology; fundamentals and applications. Oxford University Press, New York

Zängl G (2003) Deep and shallow south foehn in the region of Innsbruck: typical features and semi-idealized numerical simulations. Meteorol Atmos Phys 83:237–261